Chapter 2
Effective Piezoelectric Coefficients d_{ij}^*: From Microgeometry to Anisotropy

Abstract Piezoelectric coefficients d_{ij} are most widespread to describe the piezoelectric effect, electromechanical properties and other related parameters. The effective piezoelectric coefficients d_{ij}^* and their links to sensitivity are discussed for piezo-active composites with various connectivity patterns. Examples of the piezoelectric sensitivity of the 2–2-type, 1–3-type, 1–1-type, 0–3-type, and 3–β composites based on ferroelectics are considered. The role of the microgeometry in forming the piezoelectric sensitivity and anisotropy of the piezoelectric coefficients d_{3j}^* is analysed. Ways to improve the piezoelectric sensitivity in terms of d_{ij}^* are discussed in connection with potential piezotechnical applications.

Among the four types of the piezoelectric coefficients that are used to describe the piezoelectric effect, electromechanical properties and other related parameters [1–5] in a piezoelectric medium, the piezoelectric coefficients d_{ij} from (1.6) to (1.7) play an important role. In the historical sense, these piezoelectric coefficients enabled the study of the direct and converse piezoelectric effects within a relatively short time range in the 1880s and demonstrate important relations between the electric and elastic responses of dielectrics under the application of external fields [1, 2]. Examples of the sensor or actuator performance and energy-harvesting characteristics of piezoelectric devices [4–8] have been studied taking into account the piezoelectric coefficients d_{ij}. They play a vital role in the study of the performance of poled FEs by piezoresponse force microscopy [9], in forming the figures of merit of hydrophones [4, 10] and related hydroacoustic devices. Based on knowledge of the d_{ij} values, one can find implicit links between the piezoelectric performance and electromechanical coupling of the piezoelectric medium, for example, see (1.16), as well as important interrelations between the four types of its piezoelectric coefficients [see, for instance, (1.20)–(1.23)] in terms of the electromechanical properties. In piezo-active composites, these coefficients are regarded as ‘effective’ properties [8, 10–12] and depend on the properties of components, orientations of their main crystallographic axes, the connectivity and microgeometry of the composite, poling conditions, technological factors, etc. [12–14].

V. Y. Topolov et al., *Piezo-Active Composites*, Springer Series
in Materials Science 271, https://doi.org/10.1007/978-3-319-93928-5_2

In this chapter we discuss examples of the effective piezoelectric coefficients d_{ij}^* and their links to the PS of piezo-active composites. We also highlight examples of the anisotropy of the piezoelectric coefficients d_{ij}^* in specific composites and their advantages over poled FCs, especially highlighting the PS along specific directions of energy conversion.

2.1 2–2-Type Composites

2.1.1 2–2 Ceramic/Polymer Composites

Since the 1970s, two-component composites consisting of FC and polymer components have been studied and manufactured for various applications [4, 8, 10, 15, 16]. Usually a FC/polymer composite is formed by combining the high piezoelectric performance of a poled FC component with the beneficial mechanical properties of a polymer component [4, 15–18]. By correctly combining the properties of the FC and polymer components and tailoring the microgeometric features, the composite can achieve specific advantages [10, 14–18] over the FC component.

The 2–2 FC/polymer composite system is widespread [10, 15–18] due to its simple laminar microgeometry and electromechanical properties. We remind the reader that the '2' index in the connectivity formula '2–2' means that the first (or second) component of this composite is distributed continuously along two co-ordinate axes [15], and the component with the higher piezoelectric activity is assumed on the first position in the formula. We will consider the 2–2 composite as a system of layers of two components, and these layers are distributed regularly along one of the co-ordinate axes. The poling direction of each FC layer and the composite sample as a whole can be chosen to be either perpendicular (Fig. 2.1) or parallel (Fig. 2.2) to the system of interfaces that separate the FC and polymer layers. In some specific cases it is possible that the poling direction of the ferroelectric polymer component can differ from the poling direction of the FC component, but in the majority of cases, the polymer is inactive and is considered as a piezo-passive component [10–12, 17, 18]. Taking into account the mutual orientation of the poling axis and interfaces, specialists often term the 2–2 composites [10, 15] 'series-connected' (Fig. 2.1) or 'parallel-connected' (Fig. 2.2).

There are many methods suitable for manufacturing the 2–2 FC/polymer composites; see, for example, work [10, 17, 18]. Rapid prototyping methods (or solid freeform fabrication) [17–19] are effective for the manufacture of fine-scale 2–2 and other FC-based composites using computer-aided design. These methods are also suitable to manufacture 2–2 composites with a volume-fraction gradient, with curved FC skeletons and with a specific orientation of the layers with respect to the poling direction [17, 18].

The simplicity of the 2–2 structure, as shown in Figs. 2.1 and 2.2, and the possibility of varying and tailoring the volume fractions of the components in a

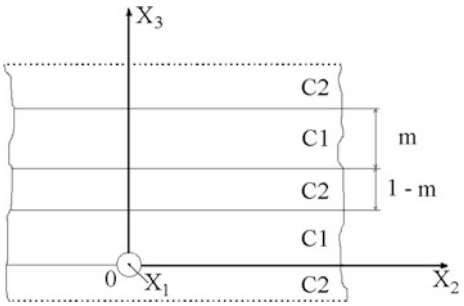

Fig. 2.1 Schematic of the 2–2 series-connected composite. m and $1 - m$ are volume fractions of components C1 and C2, respectively. $(X_1X_2X_3)$ is the rectangular co-ordinate system. In a case of the FC/polymer composite, it is assumed that OX_3 is the poling axis (reprinted from monograph by Topolov and Bowen [10], with permission from Springer)

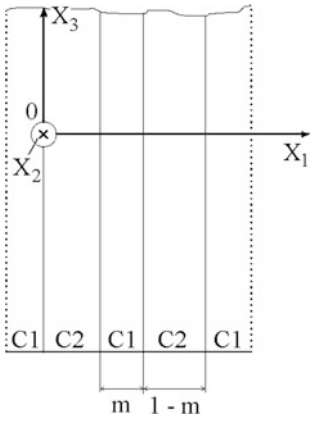

Fig. 2.2 Schematic of the 2–2 parallel-connected composite. m and $1 - m$ are volume fractions of components C1 and C2, respectively. $(X_1X_2X_3)$ is the rectangular co-ordinate system. In a case of the FC/polymer composite, it is assumed that OX_3 is the poling axis (reprinted from monograph by Topolov and Bowen [10], with permission from Springer)

wide range [10, 11, 17, 18] enable the manufacture and design of materials with extreme values of a variety of effective parameters concerned with the piezoelectric effect. For example, in the case of 2–2 series-connected FC/polymer composites based on PZT-type FCs, the non-monotonic volume-fraction dependence of the thickness ECF $k_t^* = e_{33}^* / \left(c_{33}^{*D} \varepsilon_{33}^{*\xi} \right)^{1/2}$ [see (1.17) in the similar form for a piezoelectric medium], piezoelectric coefficient e_{31}^* and dielectric permittivity $\varepsilon_{11}^{*\sigma}$ in the stress-free condition exhibit maxima [10, 11, 20], where e_{3j}^* is the piezoelectric coefficient, c_{33}^{*D} is elastic modulus measured at electric displacement D = const and $\varepsilon_{33}^{*\xi}$ is dielectric permittivity measured at mechanical strain ξ = const. The

piezoelectric coefficient e_{31}^* can pass through a value of zero and reach max $e_{31}^* > 0$ [11] even at negative values of the piezoelectric coefficient $e_{31}^{(n)}$ of the FC and polymer components. In the parallel-connected composites, the thickness ECF k_t^*, and hydrostatic (or hydrophone) piezoelectric coefficients

$$d_h^* = d_{33}^* + d_{32}^* + d_{31}^* \quad \text{and} \quad g_h^* = g_{33}^* + g_{32}^* + g_{31}^*, \tag{2.1}$$

and squared hydrostatic figure of merit

$$(Q_h^*)^2 = d_h^* g_h^* \tag{2.2}$$

pass through maxima [10, 21].

To predict the effective electromechanical properties and related parameters of the 2–2 composite, we assume that its layers have a large length in the OX_1 and OX_2 directions (Fig. 2.1) or in the OX_2 and OX_3 directions (Fig. 2.2). The interfaces separating these layers are considered planar, with perfect bonding between the adjacent layers.

To determine the effective electromechanical properties of the 2–2 composite, we apply the matrix method [10, 22]. The electromechanical constants of the nth component of the composite are given by the 9 × 9 matrix

$$\left\| C^{(n)} \right\| = \begin{pmatrix} ||s^{(n),E}|| & ||d^{(n)}||^t \\ ||d^{(n)}|| & ||\varepsilon^{(n),\sigma}|| \end{pmatrix} \tag{2.3}$$

In (2.3) $\|s^{(n),E}\|$ is the 6 × 6 matrix of elastic compliances, $\|d^{(n)}\|$ is the 6 × 3 matrix of piezoelectric coefficients and $\|\varepsilon^{(n),\sigma}\|$ is the 3 × 3 matrix of dielectric permittivities of the first component (n = 1) and second component (n = 2), and the superscript t denotes the transposition. In this method, the aforementioned matrices of properties belong to the components that can be from any symmetry class, and below we give formulae for this general case. A matrix $\|C^*\|$ of the effective electromechanical properties of the 2–2 composite is represented as [10, 22]

$$||C^*|| = \left[\left|\left|C^{(1)}\right|\right| \cdot ||M|| m + \left|\left|C^{(2)}\right|\right| (1-m) \right] [||M|| m + ||I|| (1-m)]^{-1} \tag{2.4}$$

The structure of the $\|C^*\|$ matrix from (2.4) is similar to $\|C^{(n)}\|$ from (2.3). The effective electromechanical properties of the composite are determined from (2.4) in a long-wave approximation [10, 21, 22]. This means that any wavelength from an external field is much longer than the thickness of separate layers (C1 or C2, see Figs. 2.1 and 2.1) in the composite system. In (2.4) $\|M\|$ is the matrix related to the boundary conditions at interfaces x_i = const (i = 3 for the series-connected composite, see Fig. 2.1, or i = 1 for the parallel-connected composite, see Fig. 2.1), and $\|I\|$ is the identity matrix. We remind the reader that in (2.4) we deal with the 9 × 9 matrices only.

In a 2–2 composite with a parallel connection of layers (see Fig. 2.2), the boundary conditions at x_1 = const imply a continuity of components of mechanical stress σ_{11}, σ_{12} and σ_{13}, mechanical strain ξ_{22}, ξ_{23} and ξ_{33}, electric displacement D_1, and electric field E_2 and E_3. We then represent $\|M\|$ for interfaces x_1 = const as

$$||M|| = ||p_1||^{-1}||p_2||, \tag{2.5}$$

where the matrix

$$||p_n|| = \begin{pmatrix} 1 & 0 & 0 & 0 & 0 & 0 & 0 & 0 & 0 \\ s_{12}^{(n),E} & s_{22}^{(n),E} & s_{23}^{(n),E} & s_{24}^{(n),E} & s_{25}^{(n),E} & s_{26}^{(n),E} & d_{12}^{(n)} & d_{22}^{(n)} & d_{32}^{(n)} \\ s_{13}^{(n),E} & s_{23}^{(n),E} & s_{33}^{(n),E} & s_{34}^{(n),E} & s_{35}^{(n),E} & s_{36}^{(n),E} & d_{13}^{(n)} & d_{23}^{(n)} & d_{33}^{(n)} \\ s_{14}^{(n),E} & s_{24}^{(n),E} & s_{34}^{(n),E} & s_{44}^{(n),E} & s_{45}^{(n),E} & s_{46}^{(n),E} & d_{14}^{(n)} & d_{24}^{(n)} & d_{34}^{(n)} \\ 0 & 0 & 0 & 0 & 1 & 0 & 0 & 0 & 0 \\ 0 & 0 & 0 & 0 & 0 & 1 & 0 & 0 & 0 \\ d_{11}^{(n)} & d_{12}^{(n)} & d_{13}^{(n)} & d_{14}^{(n)} & d_{15}^{(n)} & d_{16}^{(n)} & \varepsilon_{11}^{(n),\sigma} & \varepsilon_{12}^{(n),\sigma} & \varepsilon_{13}^{(n),\sigma} \\ 0 & 0 & 0 & 0 & 0 & 0 & 0 & 1 & 0 \\ 0 & 0 & 0 & 0 & 0 & 0 & 0 & 0 & 1 \end{pmatrix} \tag{2.6}$$

is written in terms of the electromechanical constants of the components, and n = 1 and 2. For the series-connected 2–2 composite, we write $\|p_n\|$ that has a form similar to that in (2.6), but is concerned with the boundary conditions at x_3 = const (Fig. 2.1). We now use $\|p_n\|$ to find $\|M\|$ from (2.5) and then to calculate the full set of electromechanical constants of the composite at m = const in accordance with (2.4).

Taking the matrix elements $C^*_{ab}(m)$ from (2.4), we analyse the effective piezoelectric coefficients $d^*_{ij}(m)$ of the 2–2 FC/polymer composite, where the volume fraction of the FC component m can be varied from 0 to 1. Here we consider examples of the piezoelectric performance of the composites whereby the polymer component is piezo-passive. The polymer components that are of interest for our analysis are shown in Table 2.1. We consider the polymer components with different stiffness characteristics, but of specific interest is so-called *auxetic*

Table 2.1 Elastic compliances s_{ab} (in 10^{-12} Pa^{-1}) and dielectric permittivity ε_{pp} of piezo-passive polymers at room temperature

Polymers	s_{11}	s_{12}	$\varepsilon_{pp}/\varepsilon_0$
Araldite [22]	216	−78	4.0
Polyurethane [23]	405	−151	3.5
Elastomer [24]	3300	−1480	5.0
Polyethylene (high-density) [8, 12, 25]	1540	−517	2.3
Auxetic polyethylene [8, 12, 25]	5260	4360	2.3

polyethylene (PE) with a negative Poisson's ratio [25]. In contrast to the remaining polymers from Table 2.1, this auxetic component is characterised by elastic compliances $s_{1b} > 0$, and such an elastic behaviour distinctively influences the piezoelectric properties of the composite. Hereby we neglect a specific microgeometry of auxetic PE [25] and regard a 2–2–γ FC/auxetic polymer composite as a material with 2–2 connectivity.

The studied 2–2 FC/polymer composites are characterised by ∞mm symmetry for a series connection (Fig. 2.1) or $mm2$ for a parallel connection (Fig. 2.2). This means that the matrix of the effective piezoelectric coefficients $\|d^{*}\|$ of the composite has the form of $\|d\|$ from (1.30) (series connection) or from (1.29) (parallel connection).

Typical examples of the piezoelectric performance of the 2–2 FC/polymer composites are shown in Figs. 2.3 and 2.4. In Fig. 2.3 the volume-fraction dependences $d_{ij}^{*}(m)$ are shown for the PCR-7M-based composite, where the PCR-7M FC is characterised by the high piezoelectric activity (as shown by data in Table 1.5). In Fig. 2.4 we show the volume-fraction dependences $d_{ij}^{*}(m)$ that are related to the composite based on the modified $PbTiO_3$ FC. It can be seen from Table 1.5 that the modified $PbTiO_3$ FC materials have a moderate piezoelectric

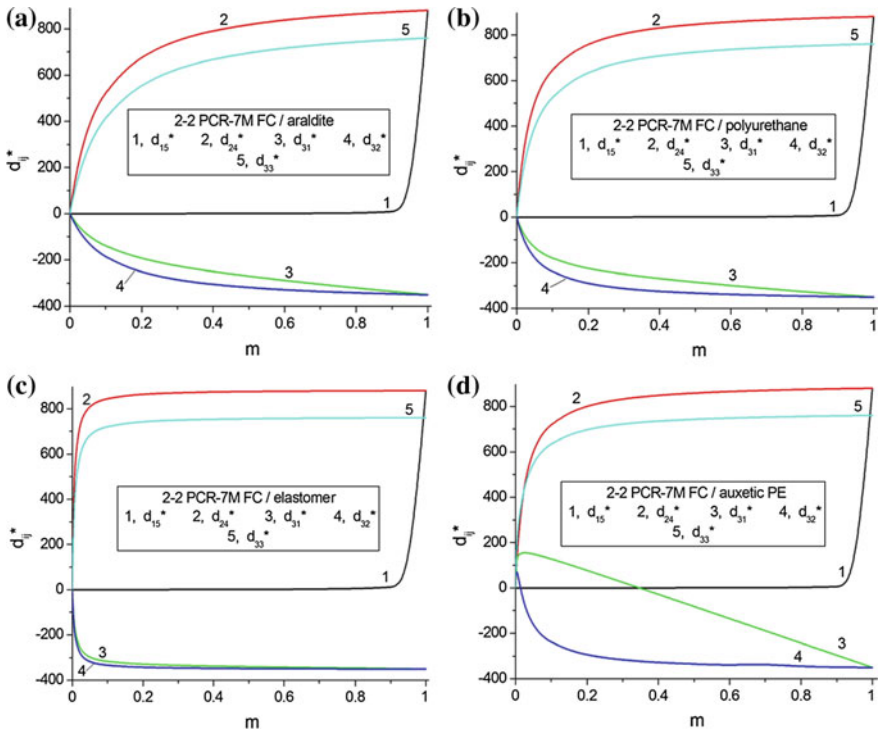

Fig. 2.3 Volume-fraction dependences of piezoelectric coefficients d_{ij}^{*} (in pC/N) of 2–2 parallel-connected PCR-7M FC/polymer composites

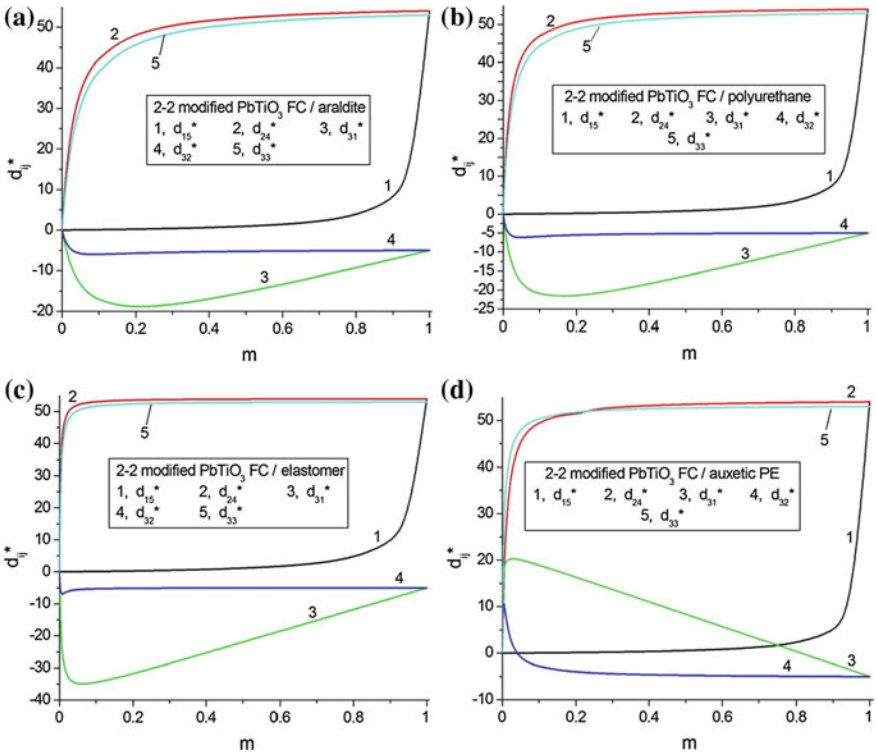

Fig. 2.4 Volume-fraction dependences of piezoelectric coefficients d_{ij}^* (in pC/N) of 2–2 parallel-connected modified $PbTiO_3$ (III) FC/polymer composites

activity (e.g., their piezoelectric coefficient d_{33} is approximately 15 times smaller than the piezoelectric coefficient d_{33} of PCR-7M), but it exhibits a large piezoelectric anisotropy, i.e., condition (1.44) holds. The graphs in Figs. 2.3 and 2.4 suggest that a change from araldite to polyurethane in the piezo-passive polymer layers of the composite does not lead to appreciable changes in the volume-fraction dependences $d_{ij}^*(m)$ (cf. Fig. 2.3a, b, as well as Fig. 2.4a, b). A change from polyurethane to elastomer in the polymer layers does however lead to distinct changes in $d_{ij}^*(m)$ (cf. Figure 2.3b, c, as well as Fig. 2.4b, c). The more remarkable changes are observed if we replace the elastomer layers with an auxetic PE, as shown in see Figs. 2.3d and 2.4d. The aforementioned changes in $d_{ij}^*(m)$ are a result of the role of the elastic properties of the polymer component. On lowering its stiffness, we achieve more rapid increase in $d_{24}^*(m)$ and $d_{33}^*(m)$, as shown by curves 2 and 5 in any graph of Figs. 2.3 and 2.4, which is a result of the piezoelectric response becoming more pronounced along the co-ordinate axes OX_2 and OX_3. As seen from Fig. 2.2, both the components are distributed continuously along these axes. In contrast to $d_{24}^*(m)$, the related shear piezoelectric coefficient $d_{15}^*(m)$ remains small in a wide m range as shown by curve 1 in any graph of Figs. 2.3 and 2.4, and

such behaviour can be accounted for by the strong influence of the interfaces x_1 = const in Fig. 2.2 on the shear piezoelectric effect. In fact, these interfaces suppress the piezoelectric polarisation along OX_1 in the presence of piezo-passive polymer layers. Changes in $d_{31}^{*}(m)$ as shown by curve 3 in any graph of Figs. 2.3 and 2.4 are concerned with the role of the interfaces x_1 = const and elastic properties of the FC and polymer components. Interrelations between their elastic compliances $s_{ab}^{(n)}$ lead to a non-monotonic volume-fraction dependence $d_{31}^{*}(m)$ (see curve 3 in Figs. 2.3d and 2.4), and in the $PbTiO_3$-based composite the elastic anisotropy of the FC component plays an important role in a wide m range.

The series-connected composites are characterised by relatively small values of $d_{3j}^{*}(m)$ at volume fractions $0 < m < 0.9$ due to the poor orientation of the layers (Fig. 2.1) with respect to the poling direction. Under an external electric field $\boldsymbol{E}\|OX_3$ a considerable depolarisation field appears in the FC layers that provide only a small contribution to the piezoelectric response of the composite along OX_3. In Table 2.2 we show examples of the volume-fraction dependences $d_{ij}^{*}(m)$ of the PCR-7M-based composite. It is clear that the lower piezoelectric activity of the modified $PbTiO_3$ FC leads to smaller values of $|d_{3j}^{*}(m)|$ in a wide m range. For instance, d_{33}^{*} = 1 pC/N at m = 0.433, and d_{31}^{*} = –1 pC/N at m = 0.910 in the 2–2 modified $PbTiO_3$ (III) FC/araldite composite with series-connected layers. In contrast to $d_{3j}^{*}(m)$, the $d_{15}^{*}(m)$ dependence follows a uniform increase with increasing m (see 4th and 7th columns in Table 2.2), and changes of the polymer component only lead to minor changes in $d_{15}^{*}(m)$. Hereby we observe the considerable shear PS, especially at $m > 0.3$. This is a result of the orientation of the interfaces (Fig. 2.1) that do not impede the shear piezoelectric effect in the series-connected composite. The auxetic polymer component strongly influences the piezoelectric coefficient

Table 2.2 Piezoelectric coefficients d_{ij}^{*} (in pC/N) of 2–2 series-connected PCR-7M-based composites

m	d_{31}^{*}	d_{33}^{*}	d_{15}^{*}	d_{31}^{*}	d_{33}^{*}	d_{15}^{*}
	PCR-7M FC/araldite			PCR-7M FC/auxetic PE		
0	0	0	0	0	0	0
0.01	–0.0593	0.0701	16.3	–0.155	–0.136	17.0
0.02	–0.0996	0.120	32.2	–0.160	–0.135	33.7
0.05	–0.171	0.211	78.6	–0.168	–0.127	82.1
0.10	–0.232	0.297	151	–0.178	–0.107	157
0.20	–0.304	0.419	280	–0.201	–0.0589	289
0.30	–0.367	0.544	391	–0.230	0.00337	401
0.50	–0.539	0.904	573	–0.322	0.203	583
0.70	–0.917	1.72	716	–0.536	0.669	723
0.90	–2.77	5.74	832	–1.60	2.99	834
0.95	–5.51	11.7	857	–3.19	6.44	858
0.99	–25.9	56.1	876	–15.4	33.0	877

$d_{33}^{*}(m)$ at volume fractions $m < 0.3$ (6th column in Table 2.2). We observe the non-monotonic behaviour of $d_{33}^{*}(m)$ at $m \ll 1$ due to the negative Poisson's ratio of auxetic PE. At $m > 0.3$ the role of the FC component becomes more active, and $d_{33}^{*}(m)$ resembles the behaviour of that in the parallel-connected composites; see, for instance, curve 5 in Fig. 2.3 or Fig. 2.4.

In general, the studied series-connected FC-based composites are characterised by the piezoelectric coefficients d_{ij}^{*} that obey the condition

$$d_{15}^{*} = d_{24}^{*} \gg \left| d_{3j}^{*} \right| \tag{2.7}$$

at $0.01 \leq m \leq 0.99$, where $j = 1$ and 3. The parallel-connected FC-based composites demonstrate different examples of the piezoelectric performance and anisotropy (Figs. 2.3 and 2.4) which depend on the properties of both the FC and polymer components. The electromechanical properties of the FC component play a dominant role at large volume fractions ($m > 0.5$), while the properties of the polymer component strongly influences the PS and anisotropy of d_{ij}^{*} in the composite, as a rule, at $m < 0.3$.

2.1.2 2–2 Single Crystal/Polymer Composites

Interest in the piezoelectric performance of modern SC/polymer composites [10, 12, 26–28] stems from the outstanding electromechanical properties of the relaxor-ferroelectric SC component [29–36]. To the best of our knowledge, full sets of electromechanical constants have been measured on samples of only perovskite-type relaxor-ferroelectric SCs along one of the following poling directions: [001], [011] or [111] in the perovskite unit cell. Examples of the electromechanical properties of the poled PMN–xPT SCs are shown in Tables 1.3, 1.4 and 2.3, and examples of the domain arrangement in the poled state are shown in Fig. 1.2. We note that PMN–0.28PT has been the first relaxor-ferroelectric SC, for which self-consistent and full sets of electromechanical constants were measured [33] on the [001]-, [011]- and [111]-poled samples. In the single-domain state at room temperature, the PMN–0.28PT SC is characterised by $3m$ symmetry with a spontaneous polarisation vector $\boldsymbol{P}_s \| [111]$. The domain-engineered SC poled along [001] exhibits $4mm$ symmetry and has an average spontaneous polarisation vector $\boldsymbol{P}_s \| [001]$. Poling along the perovskite unit-cell [011] axis leads to the domain-engineered state [32] with $mm2$ symmetry and an average spontaneous polarisation vector $\boldsymbol{P}_s \| [011]$. Data from Tables 1.3, 1.4 and 2.3 suggest that these SCs poled along the aforementioned crystallographic directions demonstrate high piezoelectric activity resulting in large absolute values of specific piezoelectric coefficients d_{ij}. Due to this piezoelectric performance and various symmetry features, the 2–2 SC/polymer composite poled along the specific direction becomes an

Table 2.3 Elastic compliances s_{ab}^E (in 10^{-12} Pa^{-1}), piezoelectric coefficients d_{ij} (in pC/N) and dielectric permittivity ε_{pp}^σ of [111]-poled single-domain PMN–xPT SCs ($3m$ symmetry) at room temperature

Electromechanical constants	Single-domain PMN–0.28PT SC [32]	Single-domain PMN–0.33PT SC [30]
s_{11}^E	8.78	62.16
s_{12}^E	−4.90	−53.85
s_{13}^E	−0.93	−5.58
s_{14}^E	16.87	−166.24
s_{33}^E	6.32	13.34
s_{44}^E	138.69	510.98
s_{66}^E	27.4	232.02
d_{15}	2382	4100
d_{22}	−312	1340
d_{31}	−43	–90
d_{33}	97	190
$\varepsilon_{11}^\sigma/\varepsilon_0$	4983	3950
$\varepsilon_{33}^\sigma/\varepsilon_0$	593	640

attractive composite material where different variants of the PS and anisotropy of d_{ij}^* can be observed. Such a composite is also of independent interest due to a variety of shear oscillation modes [36] that do not appear in conventional FC samples because of their ∞mm symmetry.

It is assumed that the 2–2 SC/polymer composite is characterised by a regular distribution of alternating SC and polymer layers in the OX_1 direction (Fig. 2.2), and the layers are continuous in the OX_2 and OX_3 directions. In Fig. 2.2 now C1 refers to SC, and C2 refers to polymer. The effective electromechanical properties of the 2–2 SC/polymer composite are determined by means of the matrix method, as described in Sect. 2.1.1. In Sect. 2.1.2 we analyse examples of the volume-fraction dependences of the piezoelectric coefficients $d_{ij}^*(m)$ (Figs. 2.5, 2.6 and 2.7) at specific orientations of the main crystallographic axes in the SC component. Among the polymer components of interest in Table 2.1, we consider araldite as a relatively stiff polymer with a positive Poisson's ratio and an auxetic PE as a very soft polymer with a negative Poisson's ratio.

The arrangement of curves in graphs of Fig. 2.5 for the SC based composites differs from the arrangement shown in Fig. 2.3 for the PCR-7M-based composite with the high piezoelectric activity. The smaller values of $d_{15}^*(m)$ and $d_{24}^*(m)$ (curves 1 and 2 in Fig. 2.5) are related to the PMN–xSC-based composites: their SC components poled along [001] are characterised by piezoelectric coefficients d_{15} (Table 1.3) that are smaller than d_{15} of the PCR-7M FC (Table 1.5). Comparing Fig. 2.5a–c leads to an increase in $|d_{3j}^*|$ due to larger values of $|d_{3j}|$ in the PMN–0.33PT SC in comparison to the PMN–0.28PT. The PMN–0.33PT is located almost at the morphotropic phase boundary and exhibits high piezoelectric activity and

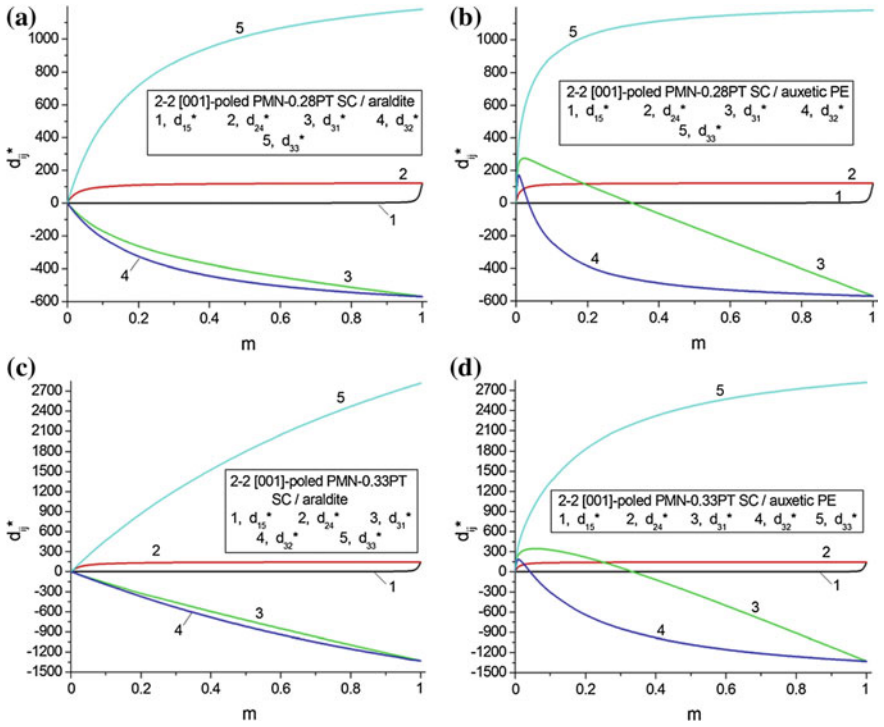

Fig. 2.5 Volume-fraction dependences of piezoelectric coefficients d_{ij}^{*} (in pC/N) of 2–2 parallel-connected [001]-poled PMN–xPT SC/polymer composites: $x = 0.28$ (**a** and **b**) and $x = 0.33$ (**c** and **d**)

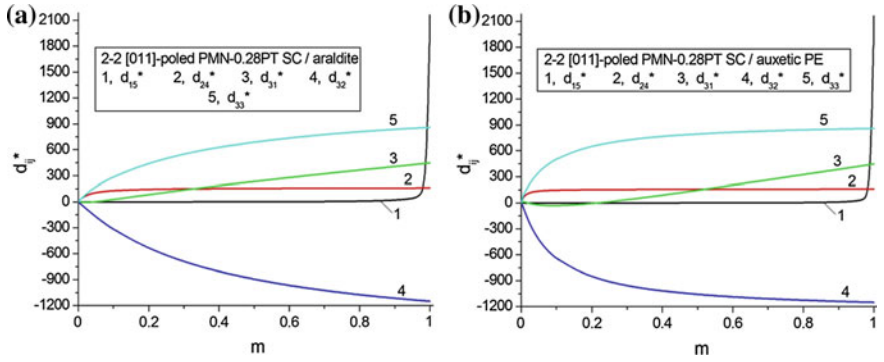

Fig. 2.6 Volume-fraction dependences of piezoelectric coefficients d_{ij}^{*} (in pC/N) of 2–2 parallel-connected [011]-poled PMN–0.28PT SC/polymer composites

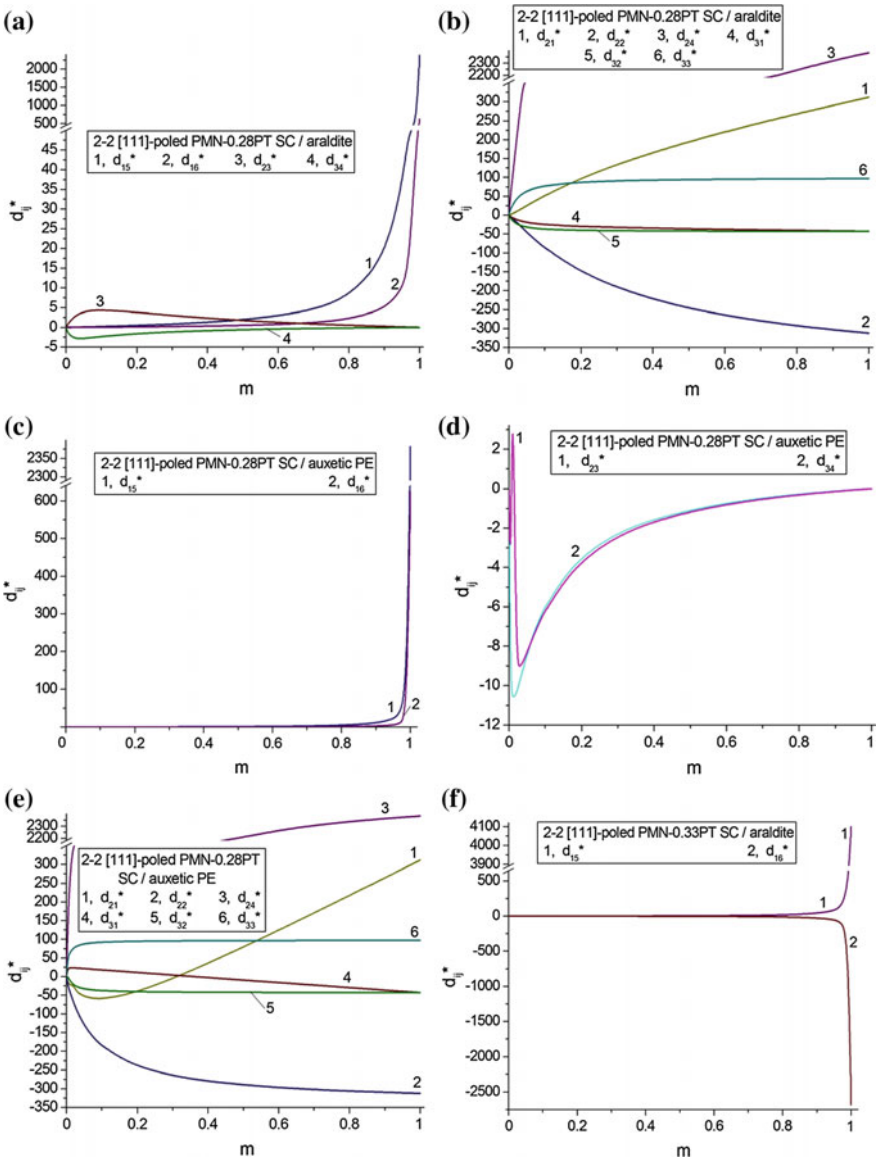

Fig. 2.7 Volume-fraction dependences of piezoelectric coefficients d_{ij}^* (in pC/N) of 2–2 parallel-connected [111]-poled PMN–xPT SC/polymer composites: $x = 0.28$ (**a**–**e**) and $x = 0.33$ (**f**–**k**)

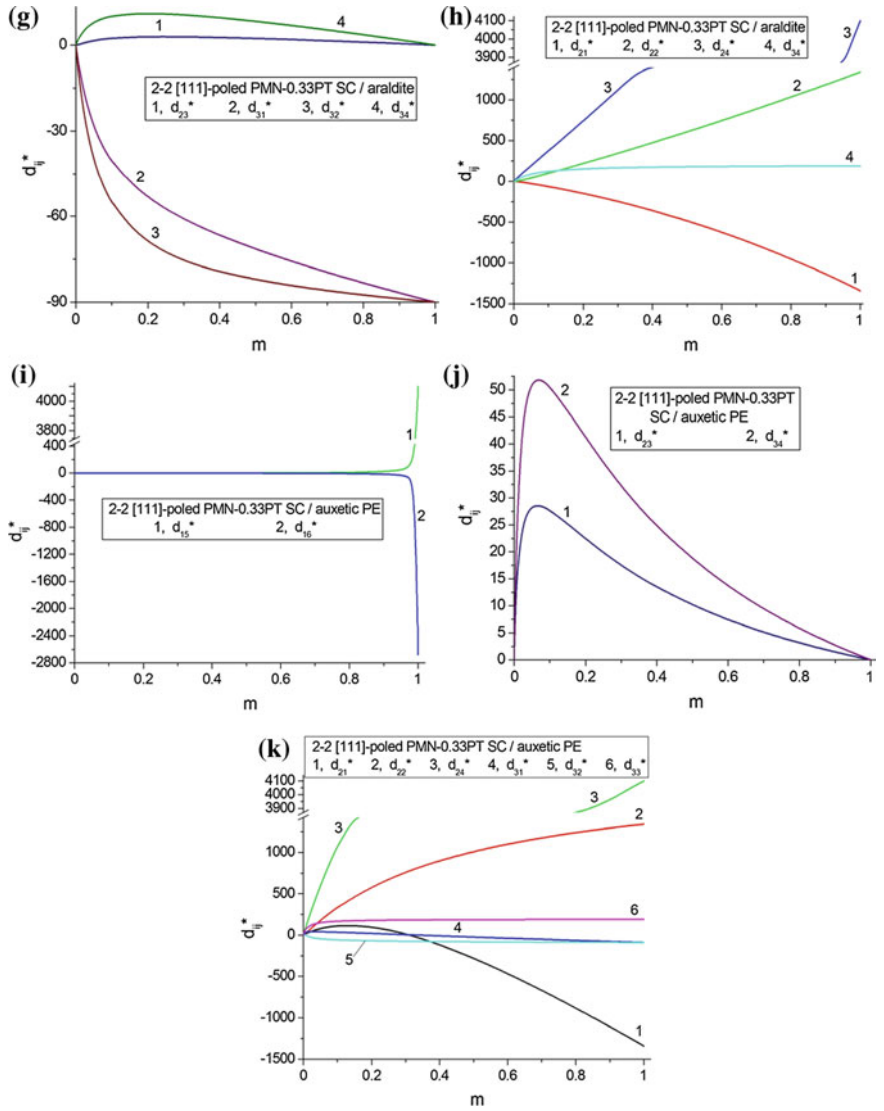

Fig. 2.7 (continued)

strong electromechanical coupling [29, 30, 36]. The auxetic polymer mainly influences the piezoelectric coefficients $d_{31}^*(m)$ and $d_{32}^*(m)$ at $m < 0.1$ (see curves 3 and 4 in Fig. 2.5b, d) irrespective of the molar concentration x in the SC component. The non-monotonic behaviour of $d_{31}^*(m)$ and $d_{32}^*(m)$ is observed at $0 < m < 0.03$, when the positive elastic compliance s_{12} of auxetic PE actively influence the transverse piezoelectric response.

In general one can state that the studied 2–2 composites based on the [001]-poled SCs are of interest due to the large values of $|d_{3j}^*|$ (Fig. 2.5) in a wide volume-fraction range.

In a case of the 2–2 composite based on the [011]-poled SC, we see minor changes in the $d_{ij}^*(m)$ dependences (Fig. 2.6) on changing the polymer component. There is the only non-monotonic $d_{31}^*(m)$ dependence in the PMN–0.28PT SC/auxetic PE composite, see curve 3 in Fig. 2.6b. This can be accounted for by the influence of the auxetic polymer component on the piezoelectric response as a result of the interfaces x_1 = const (Fig. 2.2). The piezoelectric coefficient $d_{15}^*(m)$ rapidly increases at $0.9 < m < 1$, see curve 1 in Fig. 2.6. Such a shear piezoelectric response represents an example of a '*sleeping* PS' and is strongly affected by the aforementioned interfaces x_1 = const. Due to the presence of these interfaces, the piezoelectric coefficient d_{15}^* of the composite can be considerable at very large volume fractions m of the SC component with high piezoelectric activity, and in a wide m range we observe a validity of the condition

$$d_{15}^* \ll d_{24}^* \tag{2.8}$$

(see curves 1 and 2 in Fig. 2.6). Moreover, the derivative dd_{15}^* / dm is small in the wide m range and increases at $m > 0.9$. The composite based on the [011]-poled SC is also characterised by the relation

$$d_{31}^* < d_{33}^* < \left|d_{32}^*\right| \tag{2.9}$$

as shown by curves 3–5 in Fig. 2.6. The inequality (2.9) correlates with values of the piezoelectric coefficients d_{3j} of the SC component (see Table 1.4).

The 2–2 composite based on the [111]-poled SC represents an example of the PS that depends on both the components and their volume fractions. Our analysis of the piezoelectric coefficients d_{ij}^* enables us to conclude that such a composite is described by m symmetry, and the corresponding matrix of d_{ij}^* in a case of the interfaces x_1 = const (Fig. 2.2) is given by

$$||d^*|| = \begin{pmatrix} 0 & 0 & 0 & 0 & d_{15}^* & d_{16}^* \\ d_{21}^* & d_{22}^* & d_{23}^* & d_{24}^* & 0 & 0 \\ d_{31}^* & d_{32}^* & d_{33}^* & d_{34}^* & 0 & 0 \end{pmatrix}. \tag{2.10}$$

Non-monotonic dependences of the piezoelectric coefficients $d_{ij}^*(m)$ are observed in Fig. 2.7 that are often concerned with the interfaces x_1 = const and elastic properties of the polymer component. The specific non-monotonic dependence is observed in a case when the piezoelectric coefficient $d_{ij} = 0$ for both the SC and polymer components, however $d_{ij}^* \neq 0$ is allowed for the m symmetry class, see Fig. 2.7d, j. In this situation we see relatively small deviations of d_{ij}^* from zero values at $m = 0$ and 1.

The very large values of the piezoelectric coefficient d_{15} of the [111]-poled SC (see Table 2.3) should promote large values of d_{15}^*, however the interfaces x_1 = const in the composite impede its shear piezoelectric response, and we again observe the 'sleeping PS' in the wide volume-fraction range, as shown by curve 1 in Fig. 2.7a, c, f, i. The similar 'sleeping PS' is also typical of the piezoelectric coefficient d_{16}^*, see curve 2 in Fig. 2.7a, c, f, i. In contrast to d_{15}^*, the piezoelectric coefficient d_{24}^* exhibits large values in a wide volume-fraction range irrespective of the SC and polymer component (see curve 3 in Fig. 2.7b, e, h, k), and the related shear PS may be of interest for piezoelectric sensor and actuator applications.

The large piezoelectric coefficient d_{22} of the [111]-poled PMN–0.33PT SC (see Table 2.3) leads to large values of d_{22}^* of the composite in a wide m range as shown by curve 2 in Fig. 2.7h, k, We remind the reader that the piezoelectric coefficient d_{22}^* characterises the longitudinal PS where the OX_2 axis is parallel to the interfaces x_1 = const (Fig. 2.2). In comparison to d_{22}^*, the piezoelectric coefficient d_{33}^* remains relatively small, see curve 6 in Fig. 2.7b, e, k. In the [111]-poled PMN–0.33PT SC the piezoelectric coefficient d_{33} is smaller than d_{22} by about seven times (Table 2.3), and this circumstance leads to a less favourable PS due to the piezoelectric coefficient d_{22}^* of the composite irrespective of its polymer component. Undoubtedly, the example of the pronounced longitudinal PS concerned with d_{22}^* in the PMN–0.33PT-based composite is important for sensor and actuator applications.

The [111]-poled PMN–xPT SC/auxetic PE composite is of specific interest due to the large anisotropy of the piezoelectric coefficients d_{2j}^* and changes in sgn d_{21}^*. Traditionally the poled $PbTiO_3$-type FCs and related composites exhibit a large anisotropy of d_{3j}^*: see, for instance, Table 1.5, (1.44) and work [10, 12, 37]. In the [111]-poled PMN–xPT SCs, as seen from Table 2.3, the largest longitudinal piezoelectric coefficient is d_{22}, but not d_{33}. As a consequence, the condition $d_{22}^* > d_{33}^*$ holds for the composite in a wide volume-fraction range; compare curves 2 and 6 in Fig. 2.7e or Fig. 2.7k. In the presence of auxetic polymer layer s, the effective redistribution of internal mechanical and electric fields takes place, so that conditions

$$\left| d_{22}^* / d_{2f}^* \right| \geq 5 \tag{2.11}$$

and

$$d_{21}^*(m_d) = 0 \tag{2.12}$$

can be valid. For the PMN–0.28PT-based composite, the condition (2.11) is valid at $0.178 < m < 0.449$, and $m_d = 0.312$. At $m = m_d$ the [111]-poled PMN–0.28PT SC/auxetic PE composite is characterised by the piezoelectric coefficients $d_{22}^* = -267$ pC/N and $d_{23}^* = -2.18$ pC/N, i.e., the longitudinal PS along OX_2 is dominating. For the PMN–0.33PT-based composite, the condition (2.11) is valid at $0.180 < m < 0.447$, $m_d = 0.312$, and values of $d_{22}^* = 779$ pC/N and $d_{23}^* = 17.0$ pC/N

are achieved at $m = m_d$. The piezoelectric performance at the valid condition (2.12) suggests that the studied composites have obvious advantages over the highly anisotropic $PbTiO_3$-type FCs [37] first and foremost due to the large d_{22}^{*} values. It should be added in connection with (2.11) that, in contrast to the conventional poled FCs [3, 4], electrodes on the 2–2 composite sample (Fig. 2.2) are perpendicular to the OX_2 axis. The validity of (2.11) and (2.12) opens up new possibilities of piezotechnical applications for the studied 2–2 composites. These applications can be concerned with the longitudinal oscillation modes, transducer, sensor, and other related functions of the studied piezo-active composites.

2.1.3 2–0–2 Single Crystal/Ceramic/Polymer Composites

In work [38] samples of a 2–2-type PZT FC/heterogeneous polymer composite were prepared by the adding of inorganic particles (for instance, graphite, silicon or strontium ferrite in the powder form) to each polymer layer. This use of the additives led to an improvement in specific effective parameters of the composite that is described by 2–0–2 connectivity. For instance, in the parallel-connected PZT-based composite containing strontium ferrite in the polymer layers, larger values of the ECF k_t^{*} at the thickness oscillation mode are achieved [38]. An improvement of the piezoelectric response and related parameters of the 2–2-type composites can be achieved by employing a system of 0–3 FC/polymer layers in addition to the main piezo-active component. The influence of FC inclusions in the 0–3 layer on the performance of the 2–2-type composites based on relaxor-ferroelectric SCs have been recently studied [39, 40].

Now it is assumed that the 2–0–2 composite consists of a system of parallel-connected layers of two types (Fig. 2.8), and these layers are arranged regularly along the OX_1 axis. The Type I layer is represented by a domain-engineered SC with a spontaneous polarisation $\boldsymbol{P}_s^{(1)}$ and volume fraction m. The Type II layer is regarded as a 0–3 FC/polymer composite, and the volume fraction of such layers in the composite sample is $1 - m$. The shape of each FC inclusion (see inset in Fig. 2.8) obeys the equation

$$(x_1/a_1)^2 + (x_2/a_2)^2 + (x_3/a_3)^2 = 1 \tag{2.13}$$

relative to the axes of the co-ordinate system $(X_1X_2X_3)$. In (2.13) a_1, $a_2 = a_1$ and a_3 are semi-axes of the inclusion. Its aspect ratio is $\rho_i = a_1/a_3$, and subscript 'i' denotes the inclusion. Linear sizes of each FC inclusion are much smaller than the thickness of each layer as measured along OX_1 (see Fig. 2.8). The FC inclusions in the Type II layer occupy sites of a simple tetragonal lattice with unit-cell vectors parallel to the OX_j axes. In Sect. 2.1.3 we consider the piezoelectric performance of the 2–0–2 composite that is based on either the [001]-poled SC or [011]-poled SC. Domain types in these SCs are schematically shown in Fig. 1.2.

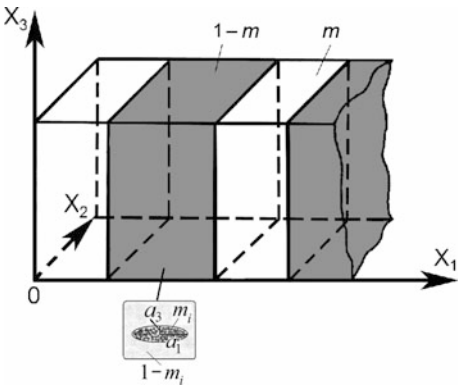

Fig. 2.8 Schematic of the 2–0–2 SC/FC/polymer composite. ($X_1X_2X_3$) is a rectangular co-ordinate system, m and $1 - m$ are volume fractions of the SC and FC/polymer layers, respectively, m_i is the volume fraction of isolated FC inclusions in the polymer medium, a_1 and a_3 are semi-axes of each inclusion (reprinted from paper by Topolov et al. [39], with permission from Taylor and Francis)

We evaluate the effective electromechanical properties of the 2–0–2 composite as follows [39]. At the first stage, the effective properties of the 0–3 FC/polymer composite in the Type II layer are determined using EFM [10] that takes into consideration an interaction between the FC inclusions. The effective electromechanical properties of the 0–3 composite are represented in the form of the 9×9 matrix as follows:

$$\left|\left|C^{(0-3)}\right|\right| = \begin{pmatrix} \left\|c^{(0-3),E}\right\| & \left\|e^{(0-3)}\right\|^t \\ \left\|e^{(0-3)}\right\| & -\left\|\varepsilon^{(0-3),\xi}\right\| \end{pmatrix}. \tag{2.14}$$

In (2.14) the superscript t denotes the transposition of the matrix. Elements of the $\|C^{(0-3)}\|$ matrix from (2.14) are found using the formula [10]

$$\begin{aligned} \left\|C^{(0-3)}\right\| = \left\|C^{(p)}\right\| + m_i\left(\left\|C^{(FC)}\right\| - \left\|C^{(p)}\right\|\right) \\ \left[\|I\| + (1-m_i)\|S\|\left\|C^{(p)}\right\|^{-1}\left(\left\|C^{(FC)}\right\| - \left\|C^{(p)}\right\|\right)\right]^{-1}. \end{aligned} \tag{2.15}$$

In (2.15), $\|C^{(FC)}\|$ and $\|C^{(p)}\|$ are matrices of the electromechanical properties of FC and polymer, respectively, $\|I\|$ is the identity matrix, and $\|S\|$ is the matrix that contains the Eshelby tensor components [41] and depends on elements of $\|C^{(p)}\|$ and the aspect ratio ρ_i. $\|C^{(FC)}\|$ and $\|C^{(p)}\|$ from (2.15) have the form shown in (2.14).

At the second stage, the effective properties of the 2–0–2 composite are evaluated using the matrix method (see Sect. 2.1.1). Hereby we use $\|C^{(0-3)}\|$ from (2.15) as the $\|C^{(2)}\|$ matrix that describes the properties of the Type II layer, and the $\|C^{(1)}\|$ matrix that characterises the properties of SC in the Type I layer. The effective electromechanical properties of the 2–0–2 composite are described by the $\|C^*\|$

matrix from (2.4). These properties are functions of the volume fraction of the SC component m, volume fraction of the FC inclusions m_i in the Type II layer and aspect ratio of these inclusions ρ_i.

Of particular interest is the combination of the soft polymer component and stiff modified $PbTiO_3$ FC in the Type II layer [39]. Differences in the elastic properties

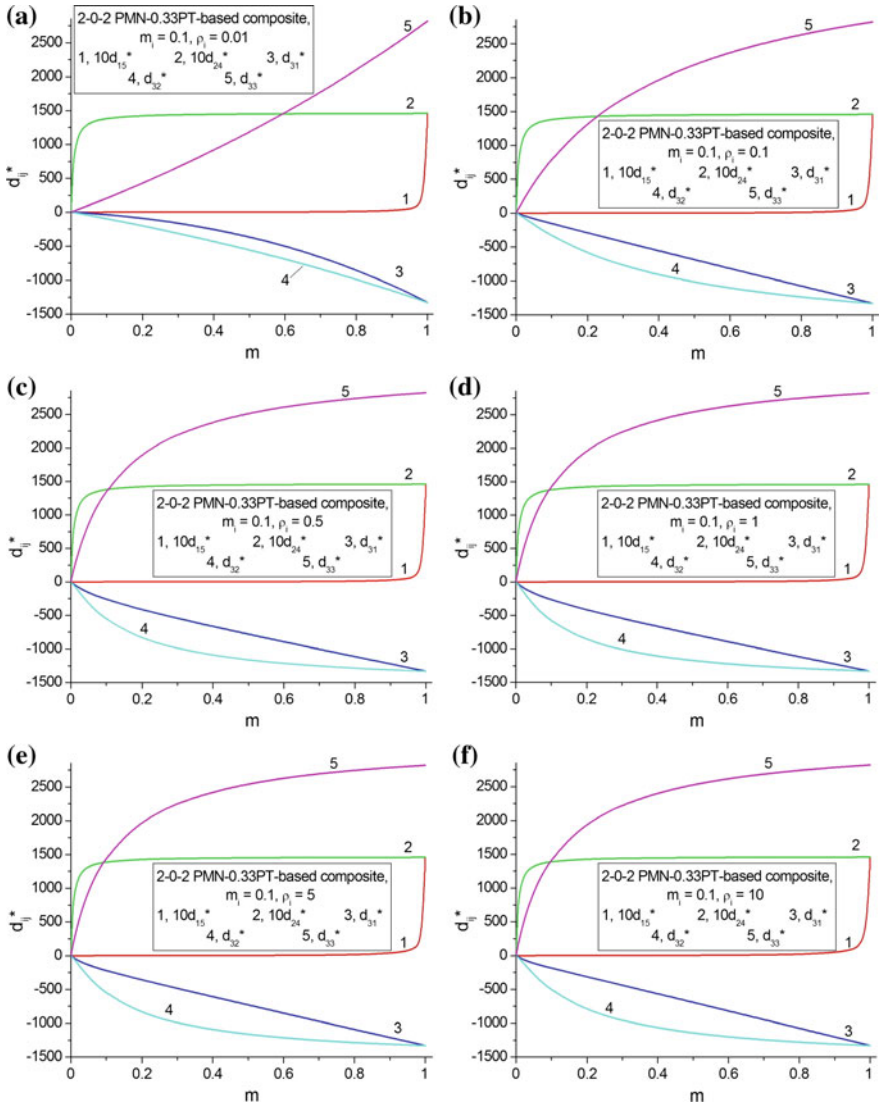

Fig. 2.9 Volume-fraction dependences of piezoelectric coefficients d_{ij}^* (in pC/N) of the 2–0–2 [001]-poled PMN–0.33PT SC/modified $PbTiO_3$ (I) FC/PE composite. The schematic of the composite is shown in Fig. 2.8

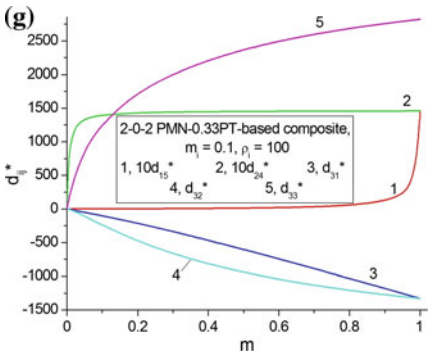

Fig. 2.9 (continued)

of the layers allow control of the dependence of the piezoelectric properties of the composite on the elastic properties and their anisotropy in the Type II layer. It is clear that changes in the elastic properties in the Type II layer are a result of changes in the volume fraction m_i and aspect ratio ρ_i of the FC inclusions therein. As follows from our evaluations, the Type II layer exhibits a low piezoelectric activity [39] compared to the SC component due to the presence of isolated FC inclusions at $0 < m_i \leq 0.3$ and $0.01 \leq \rho_i \leq 100$. The absolute values of the piezoelectric coefficients of the 0–3 modified $PbTiO_3$ FC/polymer composite are $|d_{3j}^{(0-3)}| < 10$ pC/N [39, 40], even under ideal electric poling conditions. We therefore neglect the lower piezoelectric properties of the Type II layer in the 2–0–2 composite and now consider only the piezo-active SC component, i.e., the [001]-poled domain-engineered SC (see the orientation of domains in Fig. 1.2a). Examples of the volume-fraction (m) dependence of the piezoelectric coefficients d_{ij}^* of the 2–0–2 composites are graphically represented in Figs. 2.9 and 2.10. In Figs. 2.9 and 2.10 we show the graphs for a case of a relatively small volume fraction of FC inclusions ($m_i = 0.1$) and vary their aspect ratio ρ_i in a wide range, i.e., $0.01 \leq \rho_i \leq 100$. The values of $0 < \rho_i < 1$ are related to prolate FC inclusions, and the values of $\rho_i > 1$ are related to oblate FC inclusions.

Graphs in Figs. 2.9 and 2.10 suggest that the Type II layers with the FC inclusions influence the piezoelectric properties of the studied composites in a variety of ways. The mutual arrangement of curves 1 and 2 in Figs. 2.9 and 2.10 undergo very minor changes at $0.01 \leq \rho_i \leq 100$, and this means that the shear piezoelectric effect is almost non-sensitive to changes in the microgeometry and elastic anisotropy in the Type II layer. This effect is less important in comparison to the longitudinal and transverse effects in the composite based on the [001]-poled PMN–0.33PT SC. Changes in the mutual arrangement of curves 3–5 in Figs. 2.9 and 2.10 are a result of the influence of the elastic anisotropy of the Type II layer on the piezoelectric effect (either longitudinal or transverse), and such an influence becomes more pronounced as the FC inclusions become either highly prolate or highly oblate.

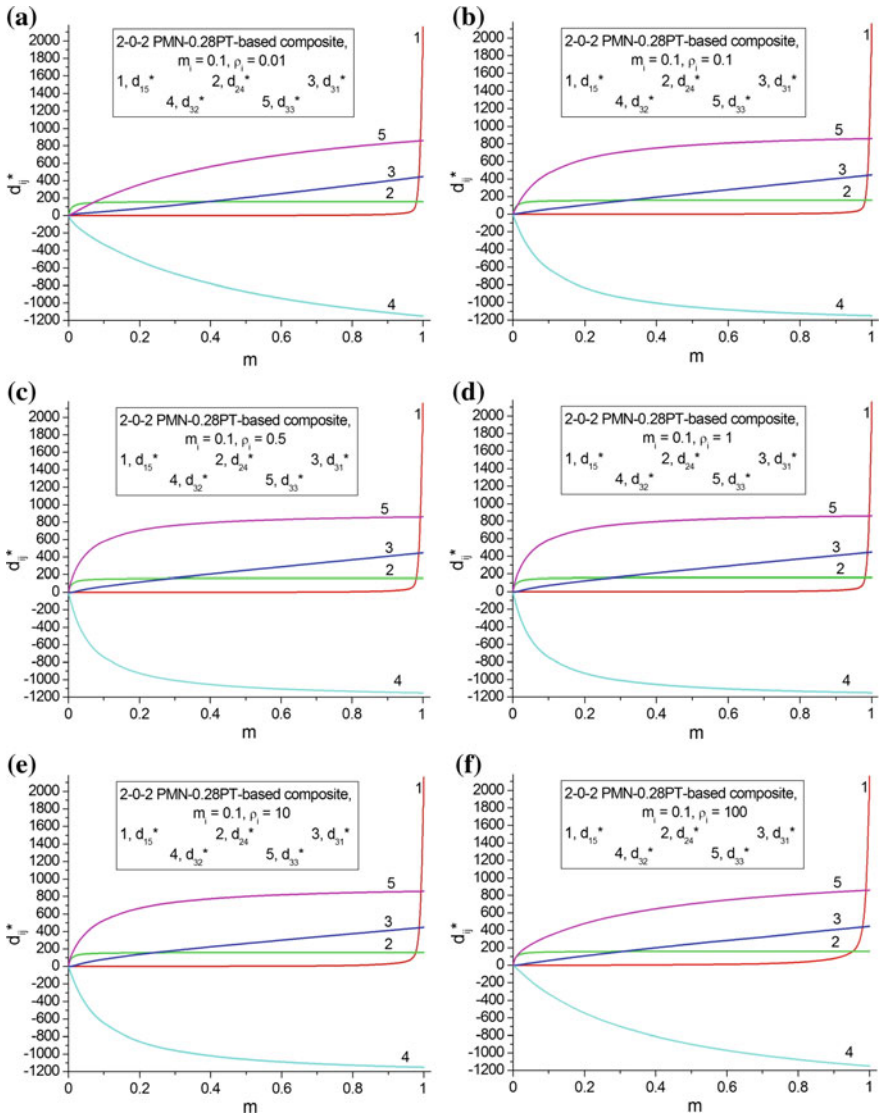

Fig. 2.10 Volume-fraction dependences of piezoelectric coefficients d_{ij}^* (in pC/N) of the 2–0–2 [011]-poled PMN–0.28PT SC/modified $PbTiO_3$ (I) FC/PE composite. The schematic of the composite is shown in Fig. 2.8

The main feature of the piezoelectric performance of the composite based on the [011]-poled PMN–0.28PT SC consists in the 'sleeping PS' concerned with the largest piezoelectric coefficient d_{15} of the SC component. The very small piezoelectric coefficient d_{15}^* in a wide m range, see curve 1 in Fig. 2.10, is due to the suppressing influence of the interfaces $x_1 = \text{const}$ (Fig. 2.8) on the shear

piezoelectric effect. The [011] poling direction leads to large values of $|d_{32}|$ of the SC component (see 2nd column in Table 1.4) and $|d_{32}^*|$ of the composite as a whole (see curve 4 in Fig. 2.10). The PMN–0.28PT-based composite is also of interest due to the relatively large values of d_{33}^*, see curve 5 in Fig. 2.10. It is obvious that the interfaces x_1 = const do not strongly influence the longitudinal piezoelectric effect in such a composite. The FC inclusions in the Type II layer influence the anisotropy of the piezoelectric coefficients d_{3j}^* to a restricted extent: there are no large changes in the mutual arrangement of curves 3–5 in Fig. 2.10 with changes of the aspect ratio ρ_i.

In our study on the 2–0–2 composites, we have used components with contrasting properties: for instance, the relaxor-ferroelectric SC with a strong shear piezoelectric effect, non-poled FC and piezo-passive polymer. The piezoelectric activity of the SC layer and the active role of the elastic subsystem in the 0–3 FC/polymer layer lead to large piezoelectric coefficients in specific ranges of the volume fraction of SC m. Such a performance of the studied 2–0–2 SC/FC/polymer composites is important for piezoelectric actuator, transducer and energy-harvesting applications concerned with specific oscillation modes.

2.2 1–3-Type Composites

In the 1–3 composite sample, a component with a higher piezoelectric activity is self-connected in one dimension, often along the poling axis, and a component with a lower piezoelectric activity, or a piezo-passive component, is self-connected in three dimensions. In fact, the 1–3 composite represents a system of long rods (component termed 'C1' in Fig. 2.11) aligned in a large matrix (component termed 'C2' in Fig. 2.11). The rods can be made of FC or ferroelectric SC, and the matrix of the composite can be made of polymer, cement, glass, etc. [4, 8, 10, 12, 17–20, 24]. The 1–3 FC/polymer composites are widespread [4, 8, 10–12, 16–18, 24, 42] for a few reasons. Among them we mention an ease of poling, available methods to manufacture high-quality composite samples and a variety of advantages for the 1–3 composite over poled monolithic FCs.

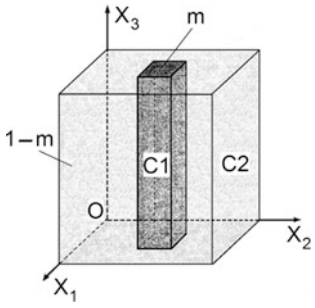

Fig. 2.11 Schematic of the 1–3 composite. m and $1 - m$ are volume fractions of components C1 and C2, respectively. $(X_1X_2X_3)$ is the rectangular co-ordinate system

The combination of the relatively low dielectric permittivity and high piezoelectric activity at small volume fractions of FC (often less than 10%) results in a significant PS associated with large values of the piezoelectric coefficient g_{33}^* of the 1–3 FC/polymer composite [10, 15, 16, 23, 24, 42]. On increasing the volume fraction of FC, the high PS of the composite is achieved due to the large piezoelectric coefficient d_{33}^* that becomes approximately equal to $d_{33}^{(1)}$ of the FC component even at its moderate volume fractions [24, 38]. Changes in the configuration of the cross section of the FC rod (C1 in Fig. 2.11) by the horizontal plane can lead to changes in the anisotropy of the piezoelectric properties of the 1–3 composite [12, 43]. Moreover, large values of its ECFs k_{33}^* and k_t^* are observed in wide volume-fraction ranges [10, 44]. These and other important parameters of the composite have stimulated intensive research into the development and manufacture of a variety of 1–3 composites in the last decades. Since the 2000s, the 1–3 relaxor-ferroelectric SC/polymer composites [8, 10, 12, 26, 27] have been advanced piezoelectric materials due to their high effective parameters and outstanding electromechanical properties of the SC components; see, for instance, Tables 1.3 and 1.4.

The piezo-active 1–3 composites are also of interest due to the non-monotonic dependence of their parameters on the volume fraction of the main piezoelectric component in rods. Among the parameters exhibiting the non-monotonic behaviour, one can mention the piezoelectric coefficients d_{3j}^*, e_{33}^*, g_{3j}^*, and h_{33}^* [10, 27, 42–44], hydrostatic piezoelectric coefficients d_h^* and g_h^* [4, 10, 24, 42, 43], thickness ECF k_t^* [10, 26, 42, 44], hydrostatic ECF k_h^* [8, 12, 23], and squared hydrostatic figure of merit $(Q_h^*)^2$ [10, 24, 44]. Of independent interest are the orientation effects [12, 45, 46] and aspect-ratio effects [47, 48] which enable us to improve some effective parameters of the 1–3-type composites based on relaxor-ferroelectric SCs. The main methods that can be applied to predict the effective electromechanical properties and related parameters of the 1–3-type composites are the matrix method, EFM and FEM [10, 22, 24, 43–48].

In Sect. 2.2 we analyse relations between the composite microgeometry and PS of various composites that are based on either FCs or ferroelectric SCs. Some modifications of the matrix and related examples of the PS will be discussed in the context of improving the performance of the composites for specific piezotechnical applications.

2.2.1 1–3 Ceramic/Polymer Composites

Since the 1980s, the 1–3 FC/polymer composite is of great interest as a heterogeneous material that combines the high PS, large figures of merit, ECFs, and other parameters [10, 11, 15, 24]. In Sect. 2.2.1 we show examples of the PS concerned with the piezoelectric coefficients d_{ij}^* of a few FC-based composites. Among the FC components of interest, as earlier, we choose the PCR-7M FC with large values of

$|d_{ij}|$ and the modified $PbTiO_3$ FC with a large anisotropy of d_{3j} (see data in Table 1.5). The polymer components that can form the matrices in the 1–3 composites are listed in Table 2.1. When using auxetic PE as a matrix component, we do not specify the connectivity pattern in the microporous polymer matrix [25] of the related composite (it should then be described by the formula 1–3–γ). In our study this composite is described by 1–3 connectivity.

It is assumed that the long FC rods (component termed 'C1' in Fig. 2.11) are arranged periodically in the large polymer matrix (component termed 'C2' in Fig. 2.11). Centres of symmetry of the bases of the FC rods form a square lattice in the (X_1OX_2) plane of the rectangular co-ordinate system $(X_1X_2X_3)$ shown in Fig. 2.11. The remanent polarisation vector of the FC rod is $\boldsymbol{P}_r^{(1)} \uparrow\uparrow OX_3$. The full set of electromechanical constants of the 1–3 composite with the square cross section rods is evaluated by means of either the matrix method [10, 22] or FEM [12, 43] via the COMSOL package [49]. The boundary conditions involve components of electric and mechanical fields at the rod—matrix interface. In FEM the rectangular representative unit cell, containing the FC rod that is adjusted to yield the appropriate volume fraction m of the FC component (Fig. 2.11), is discretised using triangular elements. The unknown displacement field is interpolated using second-order Lagrange shape functions, leading to a problem with approximately 120,000–200,000 degrees of freedom. Periodicity is enforced at the boundary of the rectangular representative unit cell of the composite. After solving the equilibrium problem, the effective elastic moduli $c_{ab}^{*E}(m)$, piezoelectric coefficients $e_{ij}^{*}(m)$ and dielectric permittivities $\varepsilon_{pq}^{*\xi}(m)$ of the composite are computed by means of averaging the resulting local stress and electric-displacement fields over the representative unit cell. The volume fraction m of FC can be varied from 0 to 1 due to the planar microgeometry of this composite, see Fig. 2.11. The matrix of its effective piezoelectric coefficients d_{ij}^{*} has the form similar to that shown in (1.30).

Examples of the volume-fraction dependences of d_{ij}^{*} are shown in Figs. 2.12 and 2.13. We observe the non-monotonic $d_{31}^{*}(m)$ dependence: see, for instance, curve 2 in Figs. 2.12d and 2.13. In the PCR-7M-based composite, d_{31}^{*} passes through a maximum point (see curve 2 in Fig. 2.12d) at small volume fractions m. A similar behaviour was observed for the related 2–2 composite, see curve 3 in Fig. 2.3d. Such a character of the $d_{31}^{*}(m)$ dependence is accounted for by the influence of the interface x_1 = const (both in the 2–2 and 1–3 composites) and by the active role of the auxetic polymer matrix. The condition $d_{31}^{*}(m) \approx 0$ holds at $m \approx 0.3$ (see curve 2 in Fig. 2.12d), and a large piezoelectric anisotropy is achieved, i.e., condition (1.44) holds for d_{3j}^{*} of the composite. Irrespective of the polymer component, the piezoelectric coefficient d_{15}^{*} exhibits minor changes at $m < 0.95$ (curve 1 in Fig. 2.12), and we observe the 'sleeping PS' due to the weak shear effect suppressed by the FC—polymer interfaces in the composite structure (Fig. 2.11). We remind the reader that the similar examples of the 'sleeping PS' concerned with d_{15}^{*} and planar interfaces were shown in Sect. 2.1.

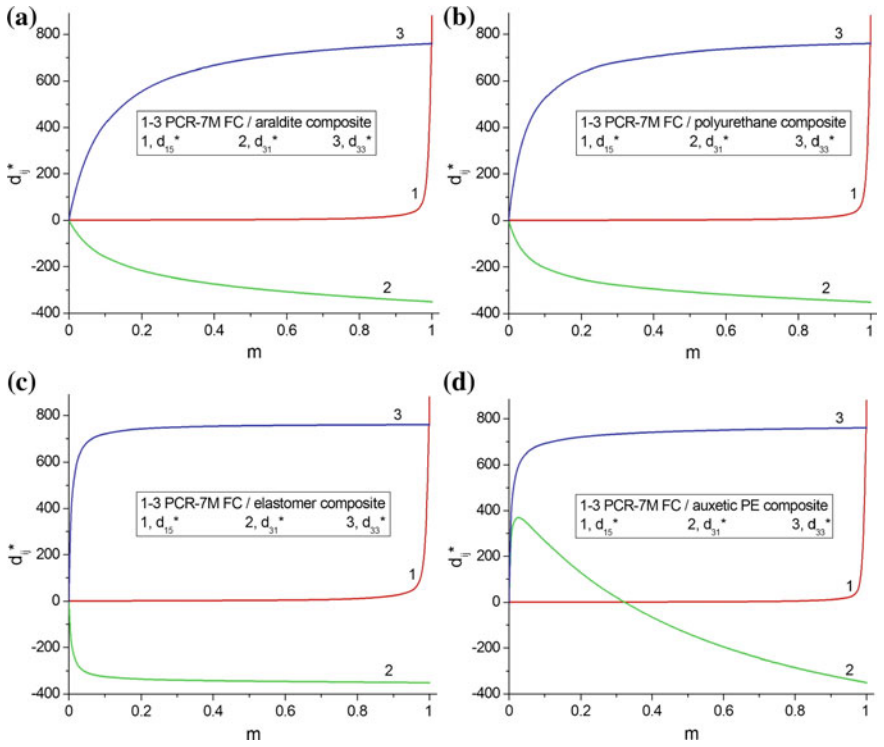

Fig. 2.12 Volume-fraction dependences of piezoelectric coefficients d_{ij}^* (in pC/N) of 1–3 PCR-7 M FC/polymer composites with square cross section rods. The schematic of the composite is shown in Fig. 2.11

In contrast to d_{15}^*, the piezoelectric coefficient d_{33}^* of the 1–3 composite is characterised by a rapid increase (see curve 3 in Fig. 2.12), and softening the polymer component promotes the larger values of d_{33}^*. This is due to the system of FC rods that are poled and distributed continuously along the OX_3 axis (see C1 in Fig. 2.11).

The 1–3 composite based on the modified $PbTiO_3$ FC demonstrates trends in the behaviour of $d_{15}^*(m)$ (curve 1 in Fig. 2.13) and $d_{33}^*(m)$ (curve 3 in Fig. 2.13) as shown in Fig. 2.12 for the PCR-7M-based composite. The non-monotonic $d_{31}^*(m)$ dependence (see curve 2 in Fig. 2.13a–c) at relatively small volume fractions m and in the presence of the polymer matrix with a positive Poisson's ratio is similar to that observed in the related 2–2 composite (see curve 3 in Fig. 2.4a–c). It is also seen that min $d_{31}^*(m)$ shifts towards the volume fraction $m = 0$ (see curve 2 in Fig. 2.13a–c) on softening the polymer matrix in the 1–3 composite or the polymer layers in 2–2 composites (see curve 3 in Fig. 2.4a–c). In both composite types, the interfaces x_1 = const play a key role in forming the lateral piezoelectric effect and strongly influence the $d_{31}^*(m)$ dependence, however the $|d_{31}^*|$ value remains fairly

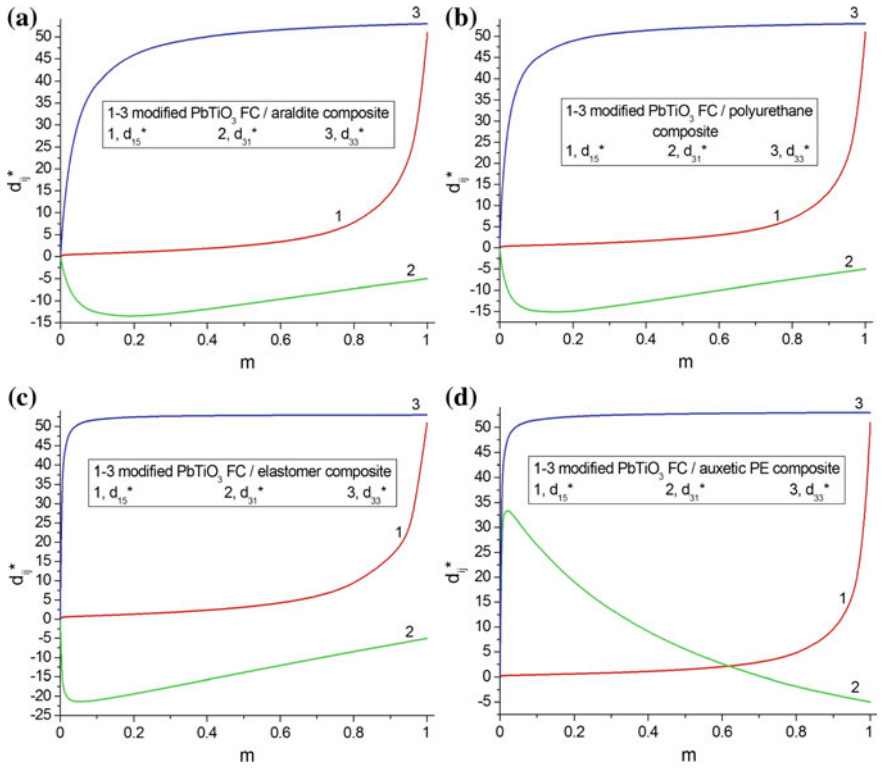

Fig. 2.13 Volume-fraction dependences of piezoelectric coefficients d_{ij}^* (in pC/N) of 1–3 modified $PbTiO_3$ (III) FC/polymer composites with square cross section rods. The schematic of the composite is shown in Fig. 2.11

small in comparison to $|d_{31}^*|$ of the aforementioned PCR-7M-based composite. It is striking that the auxetic polymer matrix leads to an increase in $d_{31}^*(m)$ in the modified $PbTiO_3$ FC/auxetic PE composite by approximately 6.5 times in comparison to $|d_{31}|$ of FC. As follows from our analysis, max $d_{31}^*(m)$ appears at a volume fraction $m \ll 1$ (see curve 2 in Fig. 2.13d) due to the active influence of elastic properties of the auxetic polymer component on the piezoelectric performance of the composite.

The 1–3 FC-based composites are also studied to show the role of the pillar effect in forming the effective properties and their anisotropy [12, 43]. The pillar effect in the 1–3 composite mainly means the influence of the cross section of the piezoelectric rod on the performance of the composite. In Sect. 2.2.1 we discuss a performance of a 1–3 FC/polymer composite with elliptical cross sections of rods (Fig. 2.14) in the (X_1OX_2) plane that is perpendicular to the poling axis OX_3. This 1–3 composite has a cellular structure and a regular distribution of FC rods in the large polymer matrix.

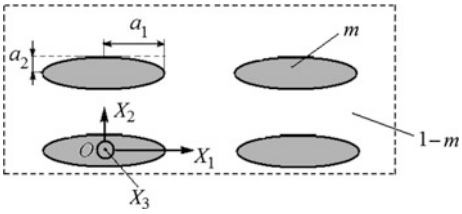

Fig. 2.14 Cross section of the 1–3 FC/polymer composite by the X_1OX_2 plane. ($X_1X_2X_3$) is the rectangular co-ordinate system, a_1 and a_2 are semi-axes of the ellipse, m is the volume fraction of FC, and $1 - m$ is the volume fraction of polymer (reprinted from paper by Topolov and Bisegna [43], with permission from Springer)

Cross sections of the FC rods by the (X_1OX_2) plane of the rectangular co-ordinate system ($X_1X_2X_3$) (Fig. 2.14) are described by the equation

$$(x_1/a_1)^2 + (x_2/a_2)^2 = 1 \tag{2.16}$$

relative to the axes of the rectangular co-ordinate system ($X_1X_2X_3$). Semi-axes of the ellipse a_f ($f = 1$ and 2) from (2.16) are constant in the whole composite sample. Centres of symmetry of these ellipses are arranged periodically on the OX_1 and OX_2 directions. The remanent polarisation vector of each FC rod is $\boldsymbol{P}_r^{(1)} \uparrow\uparrow OX_3$. It is assumed that the FC rods are aligned along the OX_3 axis (like the C1 rods in Fig. 2.11), and the height of each rod obeys the condition $h \gg a_f$.

The effective electromechanical properties of the 1–3 composite with elliptical cross sections of its rods are determined in the long-wave approximation [8, 12, 43] within the framework of the FEM via the COMSOL package. The rectangular representative unit cell, containing the FC rod in the form of an elliptical cylinder with semi-axes a_f adjusted to yield the appropriate volume fraction m of the FC component (Fig. 2.14), is discretised using triangular elements. The unknown displacement field is interpolated using second-order Lagrange shape functions, leading to a problem with approximately 120,000–200,000 degrees of freedom. The number of the degrees of freedom depends on the ratio of semi-axes $\eta = a_2/a_1$. Periodicity is enforced at the boundary of the rectangular representative unit cell of the composite. After solving the equilibrium problem, the effective elastic moduli $c_{ab}^{*E}(m, \eta)$, piezoelectric coefficients $e_{ij}^*(m, \eta)$ and dielectric permittivities $\varepsilon_{pq}^{*\zeta}(m, \eta)$ of the composite are computed by means of averaging the resulting local stress and electric-displacement fields over the representative unit cell. We add that the volume fraction m and the ratio of semi-axes η are varied [43] in ranges $0 < \eta \leq 1$ and $0 < m < \pi/4$, respectively. The limiting case of $\eta = 0$ corresponds to a 2–2 parallel-connected composite, and the limiting case of $\eta = 1$ is relevant to a circular rod cross section and the 1–3 connectivity pattern. The limiting case of the volume fraction $m = \pi/4$ is related to a system of the rods touching each other.

As follows from our analysis, the matrix of the piezoelectric coefficients d_{ij}^* of the 1–3 FC/polymer composite at $0 < \eta < 1$ has the form shown in (1.29), and at

$\eta = 1$ the matrix of d_{ij}^* is similar to that in (1.30). In a wide volume-fraction range, the shear piezoelectric coefficients d_{15}^* and d_{24}^* obey conditions

$$d_{15}^* \ll \left|d_{3j}^*\right| \quad \text{and} \quad d_{24}^* \ll \left|d_{3j}^*\right| \quad \text{at } m = \text{const}, \tag{2.17}$$

where $j = 1$, 2 and 3. We observed a similar 'sleeping PS' as a result of the very weak shear piezoelectric effect in the 1–3 PCR-7M-based composites with circular cylindrical rods, see curves 1 in graphs of Fig. 2.12. Changes in the piezoelectric coefficients $d_{3j}^*(m, \eta)$ at $0 \leq m \leq 0.7$ and $0.01 \leq \eta \leq 1$ are graphically represented in Fig. 2.15. Trends in changes of d_{3j}^* are similar to that shown in Fig. 2.12d: the configuration of curve 2 therein resembles the configuration of curves built for d_{31}^* (Fig. 2.15a) or d_{32}^* (Fig. 2.15b) at η = const, and the configuration of curve 3 in Fig. 2.12d is similar to the configuration of curves built for d_{33}^* (Fig. 2.15c) at η = const. The auxetic polymer component with a negative Poisson's ratio strongly

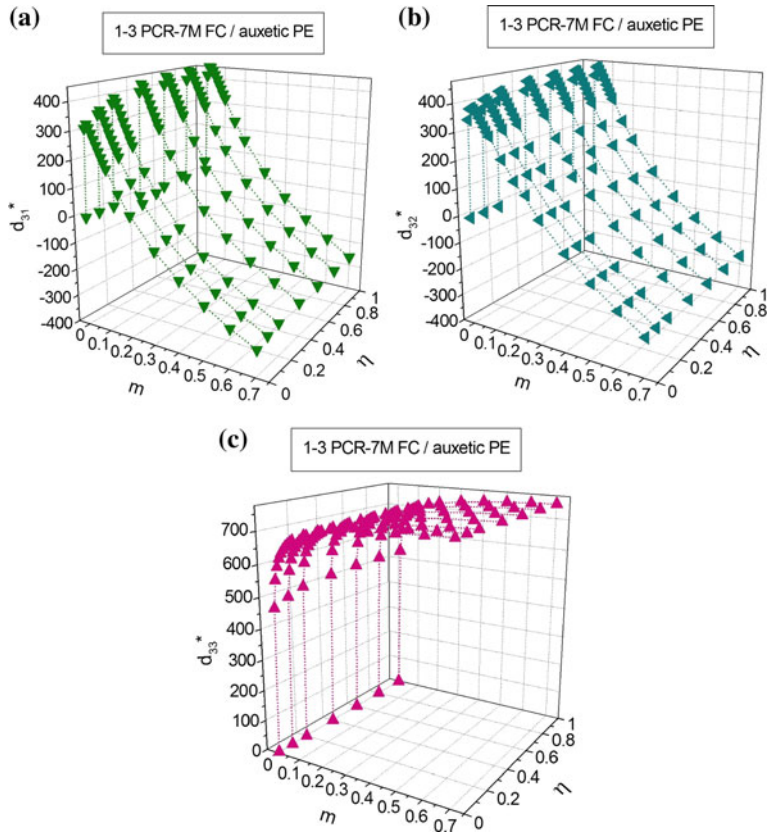

Fig. 2.15 Piezoelectric coefficients d_{3j}^* (in pC/N) of the 1–3 PCR-7M FC/auxetic PE composite with elliptical cross section rods

influences the lateral piezoelectric effect in the composite (Fig. 2.15a, b) at volume fractions $m \ll 1$. Due to the presence of the auxetic PE matrix, changes in sgn d_{31}^* and sgn d_{32}^* are observed, and this is also typical of the volume fractions $m \ll 1$, see Fig. 2.15a, b. Changes in the η value lead to the equality $d_{31}^* \approx d_{32}^*$ that holds in the wide m range. The range $0.2 < m < 0.4$ is of interest due to the large anisotropy of d_{3j}^*: we see that at increasing the volume fraction m, the condition $d_{31}^* = 0$ holds at $m = m_1$ and the condition $d_{32}^* = 0$ holds at $m = m_2 > m_1$. For the studied the 1–3 PCR-7M FC/auxetic PE composite, the difference $m_2 - m_1$ does not exceed 0.15 in the wide η range.

Figure 2.15c suggests that the longitudinal piezoelectric effect in the studied composite undergoes minor changes at varying η. Changes of the piezoelectric coefficient d_{33}^* at η = const are similar to those in the 1–3 composites wherein the polymer matrix is characterised by a positive Poisson's ratio (see, for instance, curve 3 in Fig. 2.13a–c), and the configuration of the cross section of the rod has a little influence on the $d_{33}^*(m)$ dependence. It should be added that the $d_{33}^*(m)$ dependence is similar to that related to the parallel-connected 2–2 FC/polymer composites (see curve 5 in Fig. 2.3a–c or Fig. 2.4a–c). This is accounted for by the continuous distribution of the FC component (i.e., rods in the 1–3 composite or layers in the 2–2 composite) along the OX_3 axis, see C1 in Figs. 2.2 and 2.11.

2.2.2 1–3 Single Crystal/Polymer Composites

Piezo-active 1–3 composites based on SCs of the perovskite-type relaxor-based solid solutions, e.g. PMN–xPT and PZN–xPT, are intensively studied as high-performance materials [8, 10, 12, 44, 50] and suitable [26, 27] for piezoelectric transducer and energy-harvesting applications. The main reason for the high piezoelectric performance of these composites is the outstanding electromechanical properties of the domain-engineered PMN–xPT and PZN–xPT SCs with compositions near the morphotropic phase boundary; see, for instance, the full sets of electromechanical constants of these SCs in Tables 1.3 and 1.4.

A modification of the 1–3 composite structure shown in Fig. 2.11 becomes an important factor [8, 9, 50] that influences the effective parameters and potential applications for advanced piezo-active composites. The relative simplicity of the 1–3 composite structure and possibilities for modification (such as reinforcing the polymer matrix with a third component, formation of a porous polymer matrix, etc. [9, 11]) open up possibilities to improve the PS of the 1–3-type composites.

The first example of the PS is concerned with the 1–3 composite based on the domain-engineered PMN–0.33PT SC, see graphs of d_{ij}^* in Fig. 2.16. The effective electromechanical properties of the 1–3 composite are determined by means of the matrix method, see (2.4) and work [10, 22]. It is seen that replacing the polymer component does not lead to appreciable changes of d_{15}^* (see curve 1 in Fig. 2.16). A transition from a hard polymer (araldite) to a soft polymer (elastomer) leads to a

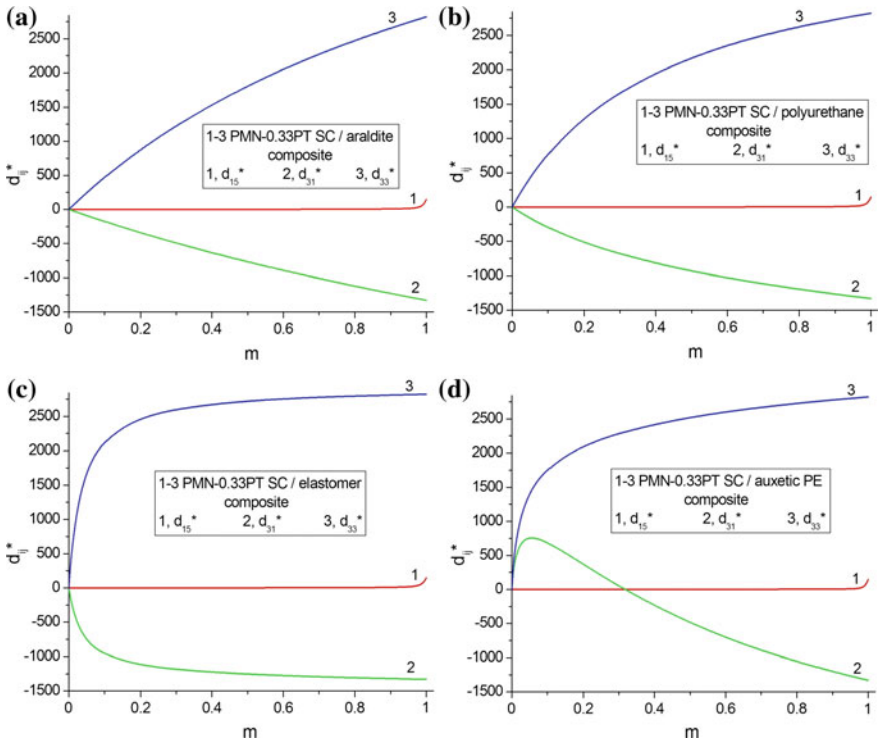

Fig. 2.16 Volume-fraction dependences of piezoelectric coefficients d_{ij}^* (in pC/N) of 1–3 [001]-poled PMN–0.33PT SC/polymer composites with square cross section rods. The schematic of the composite is shown in Fig. 2.11

more intensive increase of $|d_{3j}^*|$ at the volume fraction of SC in the range $0 < m < 0.2$ (see curves 2 and 3 in Fig. 2.16c), and the saturation of $|d_{3j}^*|$ is observed at $m > 0.6$. The auxetic polymer component strongly influences d_{31}^*, especially at $0 < m < 0.2$ (see curve 2 in Fig. 2.16d), and this effect concerned with the negative Poisson's ratio is similar to that in the 2–2 SC/auxetic PE composite (see curve 3 in Fig. 2.5b, d).

In the second example we consider a 1–3 composite based on the domain-engineered KNNTL:Mn SC. The volume-fraction dependences of d_{3j}^* of this lead-free composite (Fig. 2.17) are similar to those shown in Fig. 2.16. However a larger difference between elastic compliances of the KNNTL:Mn SC and polymer components enables us to observe the saturation of $|d_{3j}^*|$ even at $m > 0.2$ (Fig. 2.17c). The smaller values of the piezoelectric coefficients $|d_{3j}|$ of the KNNTL:Mn SC (Table 1.2) in comparison to $|d_{3j}|$ of the PMN–0.33PT SC (Table 1.3) lead to a lower PS of the lead-free composite in comparison to that based on the PMN–0.33PT SC. Nevertheless, the KNNTL:Mn-based composite may be of interest due to $d_{33}^* \approx 500$ pC/N (see curve 3 in Fig. 2.17) and $d_{31}^* = 0$

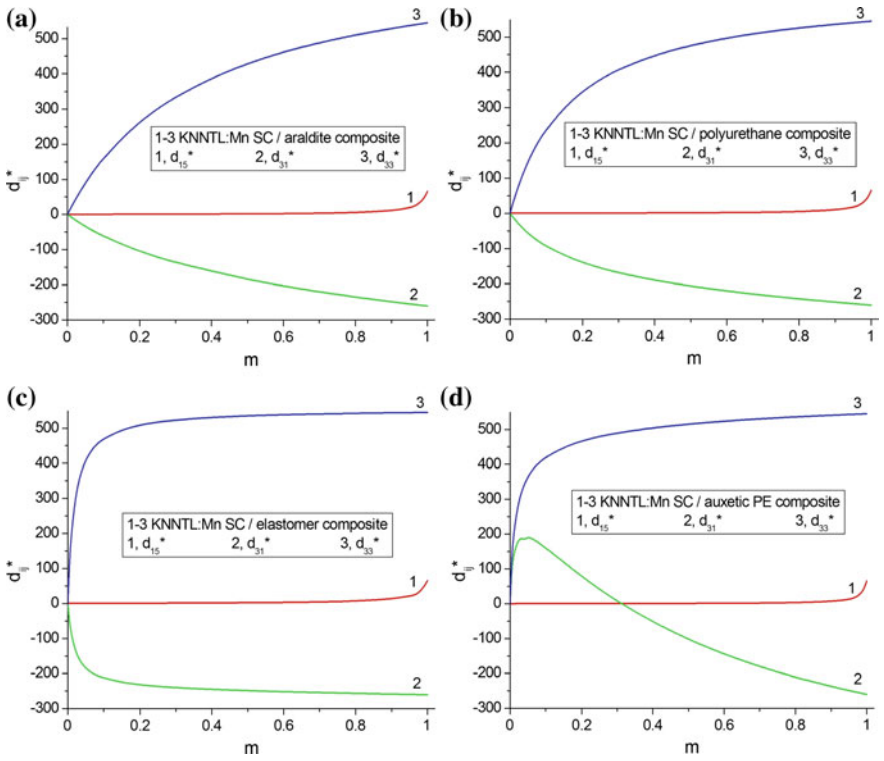

Fig. 2.17 Volume-fraction dependences of piezoelectric coefficients d_{ij}^* (in pC/N) of 1–3 [001]-poled KNNTL:Mn SC/polymer composites with square cross section rods. The schematic of the composite is shown in Fig. 2.11

(see curve 2 in Fig. 2.17d). The combination of these piezoelectric coefficients leads to the longitudinal PS that is approximately 8–9 times higher than in the highly anisotropic modified $PbTiO_3$ FCs [37] whose piezoelectric coefficients d_{3j} are known from Table 1.5. It should be noted that the value of $d_{33}^* \approx 500$ pC/N is also larger than d_{33} of many poled FCs based on Pb(Zr, Ti)O_3, see Table 1.5.

2.2.3 1–2–2 Composites Based on Single Crystals

The three-component 1–3-type composite structures consisting of FC rods and polymer layers were first studied in work [51, 52]. The piezoelectric performance of the three-component composite based on the [001]-poled PMN–0.33PT SC was first discussed in work [53]. Topolov et al. first studied a 1–3-type SC-based composite [53] wherein the matrix was laminar and comprised of two piezo-passive polymer components. Due to such a matrix, an effect of the elastic properties of the

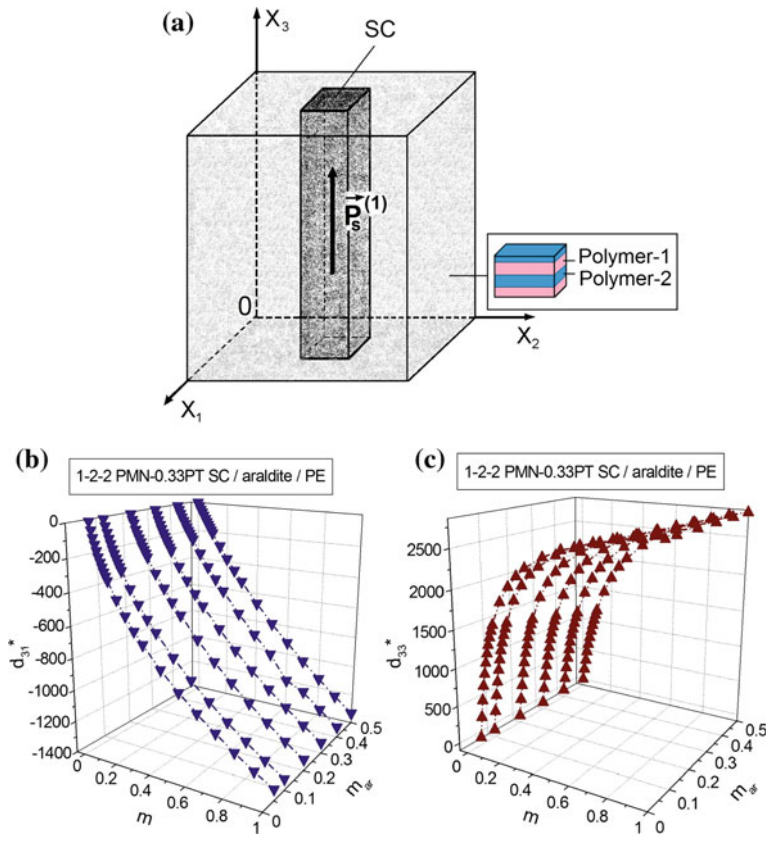

Fig. 2.18 Schematic of the 1–2–2 SC/polymer-1/polymer-2 composite (**a**) and volume-fraction dependences of piezoelectric coefficients d_{3j}^* (**b** and **c**, in pC/N) of the 1–2–2 [001]-poled PMN–0.33PT SC/araldite/monolithic PE composite with square cross section rods. In schematic a, $\boldsymbol{P}_s^{(1)}$ is the spontaneous polarisation vector of the SC component. In graphs **b** and **c**, m is the volume fraction of the SC component in the composite sample, and m_{ar} is the volume fraction of araldite in the laminar matrix

laminar polymer matrix on the performance and hydrostatic parameters of the composite based on the PMN–0.33PT SC was described in work [53].

We assume that the long SC rods are regularly distributed in the laminar matrix surrounding them (Fig. 2.18a), and a square arrangement of the rods is observed in the (X_1OX_2) plane. The main crystallographic axes of each SC rod are oriented as follows: X$\|OX_1$, Y$\|OX_2$ and Z$\|OX_3$. The layers of the two polymers are regularly distributed along the OX_3 axis (see inset in Fig. 2.18a) that is the poling axis of the composite. The composite system is described by 1–2–2 connectivity. For this composite, we first evaluate the electromechanical properties of the laminar polymer matrix (2–2 connectivity, matrix method) and then the properties of the system "Rods—laminar matrix" (1–3 connectivity, either by the matrix method or FEM).

Results based on the matrix method are shown in Fig. 2.18b, c. A difference between values of d_{3j}^{*} calculated by the matrix method and FEM does not exceed 2% in a wide m range.

The volume fraction of araldite m_{ar} in the laminar matrix influences an increase of $|d_{3j}^{*}|$ and PS of the composite with increasing m. At larger volume fractions m_{ar}, this increase becomes less intensive at $m \ll 1$. One of the main reasons for such a behaviour is related to a decrease of the elastic compliance $s_{33}^{(2)}$ of the laminar matrix on increasing m_{ar}, and this decrease strongly influences the piezoelectric effect, especially along the OX_3 axis. As is known from work [50], the combination of the polymer layers with the larger difference between their elastic constants influences the lateral piezoelectric effect in the 1–2–2 composite to a larger degree. Hereby the role of the laminar matrix is similar to the role of the system of the highly oblate pores in the porous polymer matrix [50], see Sect. 2.2.4. The aforementioned features of the PS and anisotropy of d_{3j}^{*} are to be taken into consideration at the prediction of the piezoelectric performance of the 1–3-type composites and important for some piezotechnical applications.

2.2.4 1–3–0 Composites Based on Single Crystals

The next example of the modification of the 1–3 composite structure is related to systems with 1–3–0 connectivity. This particular connectivity was studied in work [54, 55], however in [54, 55] no detailed study on the piezoelectric coefficients d_{ij}^{*} was carried out. In Sect. 2.2.4 we consider the behaviour of d_{ij}^{*} and related PS of the 1–3–0 composites based on SCs.

It is assumed that the composite shown in Fig. 2.19 contains a system of SC rods in a porous polymer matrix. The SC rods are in the form of rectangular parallelepipeds and continuous along the OX_3 axis. The SC rods have a square base and characterised by a regular square arrangement in the (X_1OX_2) plane. The main crystallographic axes X, Y, and Z of each SC rod are parallel to the following co-ordinate axes shown in Fig. 2.19: X$\|OX_1$, Y$\|OX_2$ and Z$\|OX_3$. Each SC rod is characterised by a spontaneous polarisation vector $\boldsymbol{P}_s^{(\mathbf{1})} \uparrow\uparrow OX_3$, and the OX_3 axis is the poling direction of the composite sample as a whole. The polymer matrix contains a system of spheroidal air pores that are described by the equation

$$\left(x_1/a_{1,p}\right)^2 + \left(x_2/a_{2,p}\right)^2 + \left(x_3/a_{3,p}\right)^2 = 1 \tag{2.18}$$

relative to the axes of the rectangular co-ordinate system $(X_1X_2X_3)$, and semi-axes of the spheroid from (2.18) are $a_{1,p}$, $a_{2,p} = a_{1,p}$ and $a_{3,p}$. The porous matrix is characterised by 3–0 connectivity. The air pores are regularly distributed in the polymer matrix and occupy the sites of a simple tetragonal lattice with unit-cell vectors parallel to the OX_k axes. The shape of each pore is characterised by the

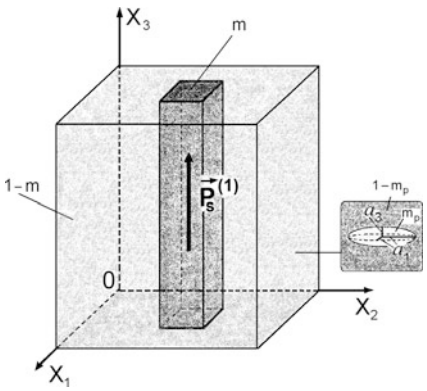

Fig. 2.19 Schematic of the 1–3–0 SC/porous polymer composite. m and $1 - m$ are volume fractions of the SC and porous polymer, respectively, m_p is the volume fraction of air in the porous polymer matrix. $\boldsymbol{P}_s^{(1)}$ is the spontaneous polarisation vector of the SC component. In the inset, a spheroidal pore with semi-axes a_f is shown schematically (reprinted from Topolov et al. [55], with permission from Elsevier)

aspect ratio $\rho_p = a_{1,p}/a_{3,p}$ that is assumed to be fixed over the composite sample. The radius or the largest semi-axis of each pore is considered to be much less than the length of the side of the square that is the intersection of the SC rod with the (X_1OX_2) plane shown in Fig. 2.19.

The effective electromechanical properties of the 1–3–0 composite shown in Fig. 2.19 are evaluated in two stages [54, 55]. During the first stage, the effective properties of the polymer matrix with spheroidal pores are determined as a function of the volume fraction of the pores (or porosity of the polymer matrix) m_p and the aspect ratio ρ_p. The corresponding calculation is based on Eshelby's concept of spheroidal inclusions in heterogeneous solids [41, 56]. The effective properties of the porous polymer medium with 3–0 connectivity are represented in the matrix form [55, 56] as follows:

$$\left|\left|C^{(3-0)}\right|\right| = \left|\left|C^{(2)}\right|\right| \left[||I|| - m_p\left(||I|| - \left(1 - m_p\right)||S||\right)^{-1}\right] \tag{2.19}$$

In (2.19) $\|C^{(2)}\|$ is the 9×9 matrix of the electromechanical properties of the polymer component, $\|I\|$ is 9×9 identity matrix, and $\|S\|$ is the 9×9 matrix that comprises components of the electroelastic Eshelby tensor [41]. The elements of $\|S\|$ depend on the aspect ratio ρ_p of the pore and on the properties of polymer. The effective properties of porous polymer are represented by

$$\left\|C^{(2)}\right\| = \begin{pmatrix} \left\|c^{(2),E}\right\| & \left\|e^{(2)}\right\|^t \\ \left\|e^{(2)}\right\| & -\left\|\varepsilon^{(2),\xi}\right\| \end{pmatrix}, \tag{2.20}$$

where $\|c^{(2),E}\|$ is the 6 × 6 matrix of elastic moduli measured at electric field E = const, $\|e^{(2)}\|$ is the 3 × 6 matrix of piezoelectric coefficients, $\|\varepsilon^{(2),\xi}\|$ is the 3 × 3 matrix of dielectric permittivities at mechanical strain ξ = const, and superscript 't' refers to the transposed matrix. The $\|C^{(3-0)}\|$ matrix from (2.19) has the structure similar to that of $\|C^{(2)}\|$ from (2.20) and $\|C^{(0-3)}\|$ from (2.14).

During the second stage of evaluations, the effective electromechanical properties of the 1–0–3 composite are calculated using either the matrix method [10, 12] or FEM [55]. Some results of calculations by means of these methods were compared in work [55]. The electromechanical properties of the 1–3–0 composite depend on the volume fractions m, m_p and aspect ratio ρ_p and are regarded as properties which are homogenised in the long-wave approximation. This means that the wavelength of an external acoustic field is much longer than the size of the SC rod in the composite sample [55].

The volume-fraction (m) dependence of the piezoelectric coefficients d_{ij}^* of the 1–0–3 composite (Fig. 2.20) shows that the main changes in the wide m range are related to d_{3j}^* (j = 1 and 3) while d_{15}^* remains small and almost constant at $0 < m < 0.9$. Thus, we observe the 'sleeping PS' at $d_{15}^* \ll d_{15}^{(1)}$ and $d\, d_{15}^*/dm \to 0$. Similar trends are observed in the 1–3 composites (see Figs. 2.12a–c, 2.16a–c and 2.17a–c) where the main piezoelectric component is characterised by a relatively small anisotropy of its piezoelectric coefficients $d_{3j}^{(1)}$ and by signs of the piezoelectric coefficients $e_{3j}^{(1)}$ [10, 12] as follows:

$$\operatorname{sgn} e_{33}^{(1)} = -\operatorname{sgn} e_{31}^{(1)} > 0. \tag{2.21}$$

A comparison of the graphs shown in Fig. 2.20 enables us to conclude that the piezoelectric coefficients d_{3j}^* at m = const undergo small changes due to the presence of both prolate ($0 < \rho_p < 1$) and spherical ($\rho_p = 1$) pores in the matrix. Distinct changes in the d_{3j}^* curves, especially at j = 3, are observed in the presence of the highly oblate pores ($\rho_p \gg 1$), see Fig. 2.20g–i. This is due to the relatively large elastic compliance $s_{33}^{(2)}$ of the porous matrix and to the considerable difference between $s_{33}^{(2)}$ and $s_{11}^{(2)}$. An increase of the porosity m_p in the matrix at ρ_p = const also leads to an increase of $s_{33}^{(2)}$, and this increase leads to a higher PS for the composite structure along the OX_3 axis. It should be added that the porous structure of the matrix in this composite system enables one to vary its piezoelectric anisotropy, but only to a restricted degree. This is a result of the presence of a SC component with a small anisotropy of its piezoelectric coefficients $d_{3j}^{(1)}$, see, for instance, data on the PMN–0.33PT SC in Table 1.3. The porous polymer matrix in the 1–3–0 composite plays an important role in forming a large anisotropy of the ECFs, and relevant examples are discussed in work [55].

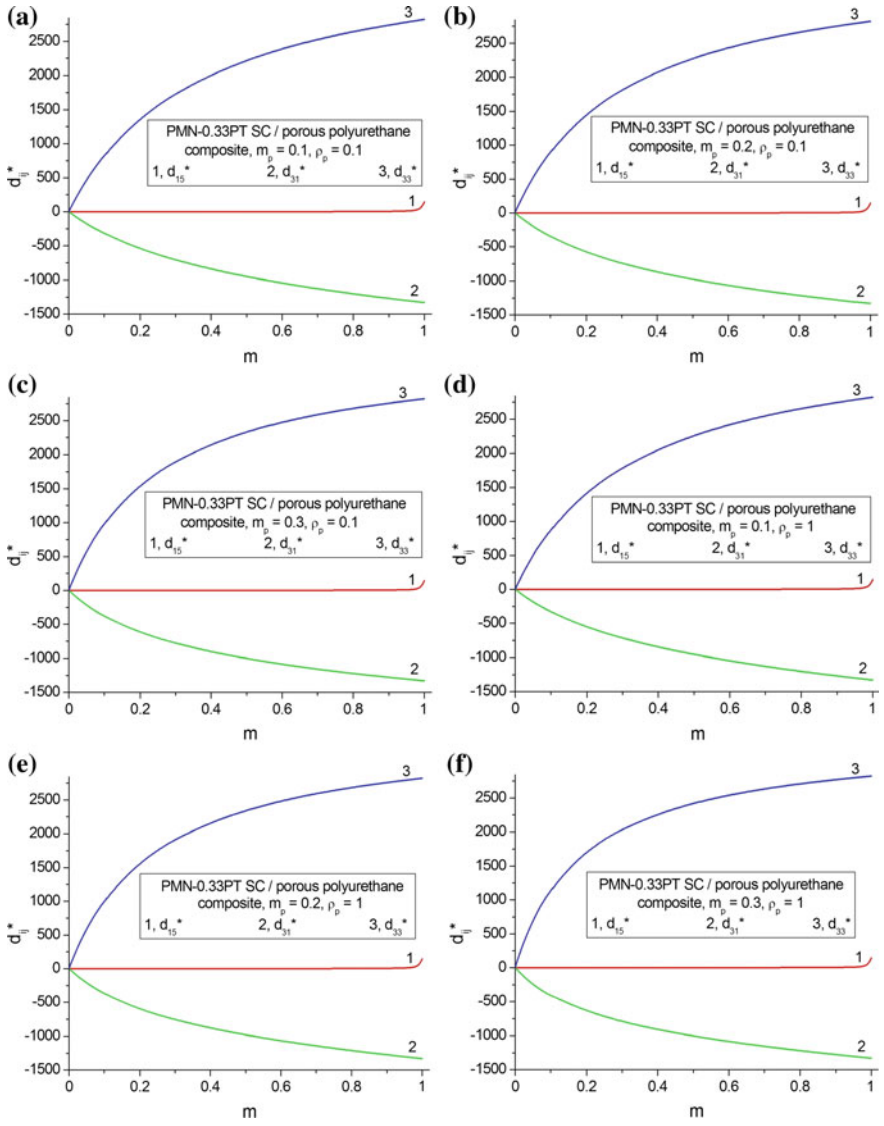

Fig. 2.20 Volume-fraction dependences of piezoelectric coefficients d_{ij}^{*} (in pC/N) of the 1–3–0 [001]-poled PMN–0.33PT SC/porous polyurethane composite with square cross section rods. The schematic of the composite is shown in Fig. 2.19

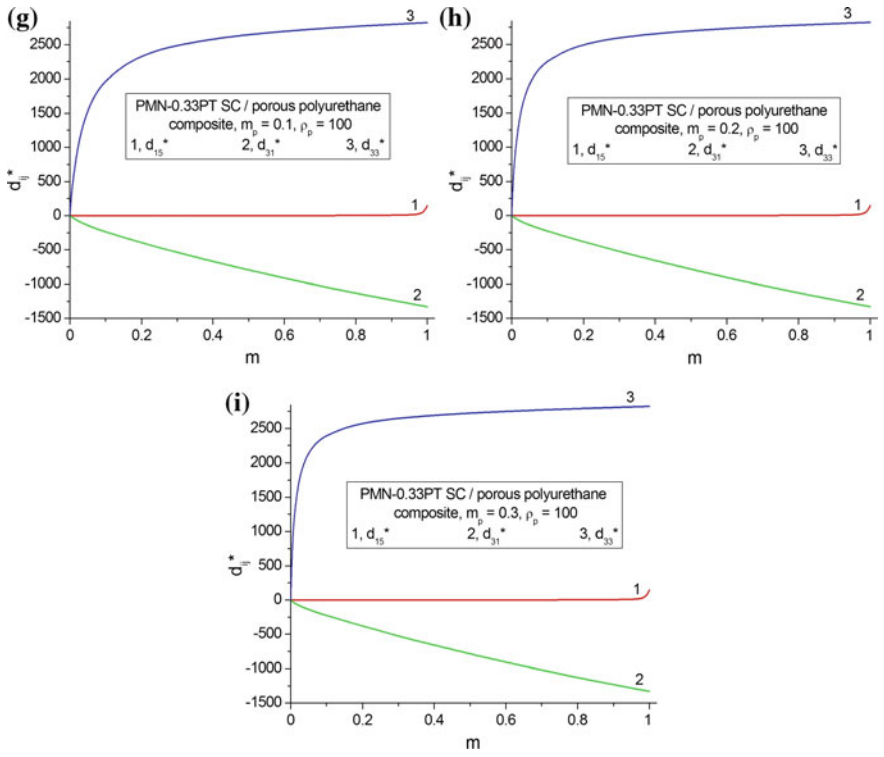

Fig. 2.20 (continued)

2.2.5 1–0–3 Composites Based on Single Crystals

The next important example of the modification of the 1–3 composite structure is concerned with the use of a 0–3 composite matrix. It is assumed that a 1–0–3 composite consists of a system of SC rods embedded in a FC/polymer matrix (Fig. 2.21). The structure of the 1–0–3 composite is similar to that shown in Fig. 2.19, however the isolated FC inclusions are regularly located in the matrix instead of the pores. The shape of each FC inclusion in the polymer matrix (see the inset in Fig. 2.19) obeys (2.13) relative to the axes of the rectangular co-ordinate system ($X_1X_2X_3$), where a_1, $a_2 = a_1$ and a_3 are the semi-axes of the FC inclusion, and $\rho_i = a_1/a_3$ is its aspect ratio. The FC inclusions occupy sites of a simple tetragonal lattice with unit-cell vectors parallel to the OX_k axes. We remind the reader that the similar 0–3 composite structure was considered in the Type II layers of the 2–0–2 SC/FC/polymer composite, see Sect. 2.1.3.

The effective electromechanical properties of the 1–0–3 composite shown in Fig. 2.21 are determined in two stages that are similar to those described in Sect. 2.2.4. However during the first stage, the effective properties of the 0–3 FC/polymer composite are evaluated within the framework of the EFM [46–48] that

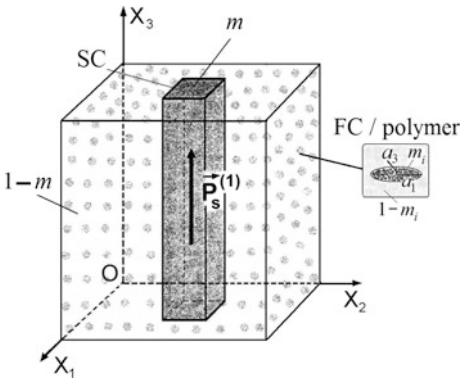

Fig. 2.21 Schematic of the 1–0–3 SC/FC/polymer composite. m and $1 - m$ are volume fractions of the SC and the FC/polymer matrix, respectively, m_i is the volume fraction of FC in the matrix, and $P_s^{(1)}$ is the spontaneous polarisation vector of the SC component. In the inset, a spheroidal FC inclusion with semi-axes a_f is shown schematically

takes into account an interaction between the FC inclusions in the polymer medium. We characterise the effective properties of the 0–3 composite by a 9×9 matrix [10]

$$\begin{aligned}\left\|C^{(0-3)}\right\| = \left\|C^{(p)}\right\| + m_i\left(\left\|C^{(FC)}\right\| - \left\|C^{(p)}\right\|\right) \\ \left[\|I\| + (1-m_i)\|S\|\left\|C^{(p)}\right\|^{-1}\left(\left\|C^{(FC)}\right\| - \left\|C^{(p)}\right\|\right)\right]^{-1}.\end{aligned} \tag{2.22}$$

$\|C^{(FC)}\|$ and $\|C^{(p)}\|$ from (2.22) characterise the properties of the FC and polymer components, respectively, and the structure of $\|C^{(0-3)}\|$, $\|C^{(FC)}\|$ and $\|C^{(p)}\|$ is similar to that of $\|C^{(2)}\|$ from (2.20). In (2.22) $\|I\|$ is the identity matrix, and $\|S\|$ is the matrix that comprises components of the electroelastic Eshelby tensor [41]. The second stage leads to the averaging of properties by means of either the matrix method or FEM [46–48]. As a result of the averaging, the effective electromechanical properties of the 1–0–3 composite are represented as functions of the volume fractions m and m_i and aspect ratio ρ_i.

By analogy with the 2–0–2 composite described in Sect. 2.1.3, we choose components with contrasting properties as follows: the [001]-poled PMN–0.33PT SC (main component, rods), modified $PbTiO_3$ FC (main component in the 0–3 matrix) and PE. Our evaluations of the properties of the 0–3 FC/polymer matrix suggest that it exhibits a low piezoelectric activity due to the presence of isolated inclusions at volume fractions of FC $0 < m_i \leq 0.3$ and aspect ratios $0.01 \leq \rho_i \leq 100$. Despite the assumption that the level of poling of the 0–3 matrix is ideal, the absolute values of its piezoelectric coefficients are relatively low whereby $|d_{3j}^{(0-3)}| < 10$ pC/N [47, 48], i.e., two orders-of-magnitude less than $|d_{3j}^{(1)}|$ of the PMN–0.33PT SC and related SCs listed in Table 1.3. Hereafter we neglect the piezoelectric activity of the 0–3 matrix in comparison to the piezoelectric activity of the SC rod and consider the FC inclusions

in the unpoled state. It is important to underline that any potential incomplete poling of the 0–3 matrix in the studied 1–0–3 composite is thereby avoided.

Graphs in Fig. 2.22 show that the FC inclusions in the polymer matrix can influence the PS of the composite even at the relatively small volume fraction

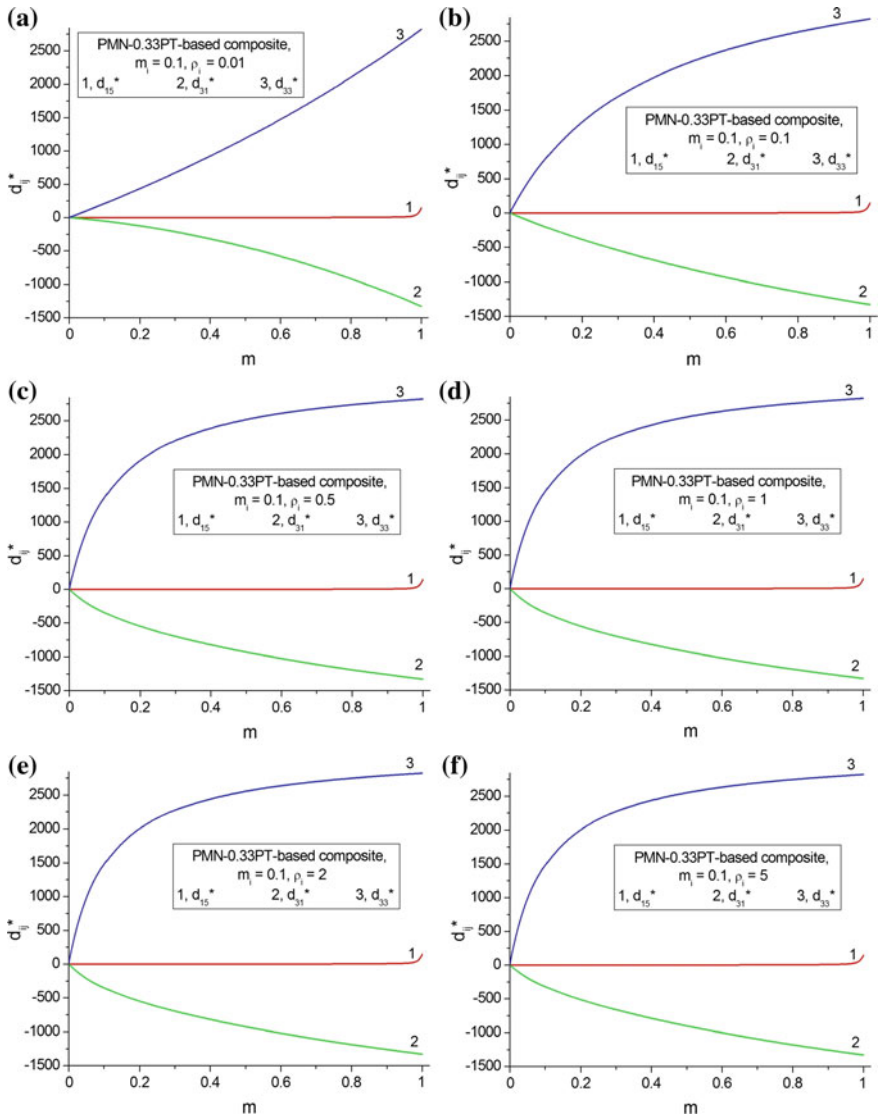

Fig. 2.22 Volume-fraction dependences of piezoelectric coefficients d_{ij}^* (in pC/N) of the 1–0–3 [001]-poled PMN–0.33PT SC/modified $PbTiO_3$ (I) FC/monolithic PE composite with square cross section rods at the volume fraction of FC $m_i = 0.1$. The schematic of the composite is shown in Fig. 2.21

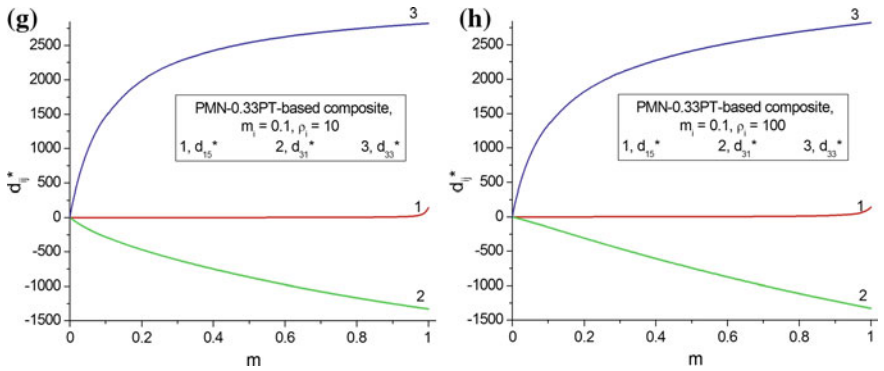

Fig. 2.22 (continued)

Table 2.4 Ratios of elastic compliances $s_{11}^{(0-3)}/s_{uv}^{(0-3)}$ of the 0–3 modified $PbTiO_3$ (I) FC/monolithic PE composite with non-poled aligned spheroidal inclusions (EFM calculations)

ρ_i	m_i	$s_{11}^{(0-3)}/s_{12}^{(0-3)}$	$s_{11}^{(0-3)}/s_{13}^{(0-3)}$	$s_{11}^{(0-3)}/s_{33}^{(0-3)}$
0.01	0.10	−3.95	−69.78	13.5
0.1	0.10	−4.22	−13.2	2.77
1	0.10	−4.86	−4.86	1.00
10	0.10	−5.14	−4.49	0.597
100	0.10	−5.65	−4.54	0.176
100	0.15	−5.67	−4.41	0.126
100	0.20	−5.68	−4.28	0.0998
100	0.25	−5.68	−4.18	0.0831
100	0.30	−5.67	−4.09	0.0709

$m_i = 0.1$. We see changes in the piezoelectric coefficients d_{3j}^* (see curves 2 and 3 in Fig. 2.22), while the piezoelectric coefficient d_{15}^* undergoes minor changes and remains small at $0 < m < 0.9$ (see curve 1 in Fig. 2.22). Such distinctions in the behaviour of the piezoelectric coefficients are observed due to the 1–3-type composite structure (Fig. 2.21) and were earlier mentioned for the 1–3 and 1–0–3 composites (see Sects. 2.2.1, 2.2.2 and 2.2.4). The changes in the piezoelectric coefficients d_{3j}^* are concerned with the changes in the aspect ratio of the FC inclusions, and the latter changes strongly influence the elastic anisotropy of the 0–3 matrix (Table 2.4). Data in Table 2.4 show that the $s_{11}^{(0-3)}/s_{uv}^{(0-3)}$ ratios undergo large changes during a transition of the FC inclusion in the 0–3 matrix from a prolate ($0 < \rho_i < 1$) to oblate ($\rho_i > 1$) shape.

An increase of the volume fraction of FC m_i leads to changes in the $s_{11}^{(0-3)}/s_{uv}^{(0-3)}$ ratios, but to a lesser degree. We show an example of such changes at $\rho_i = 100$ in Table 2.4. Figure 2.22 suggests that the piezoelectric anisotropy of the 1–0–3 composite can be varied at a relatively small anisotropy of the piezoelectric coefficients $d_{3j}^{(1)}$ of the PMN–0.33PT SC. A similar behaviour of d_{ij}^* and variations of the

piezoelectric anisotropy are observed (Fig. 2.23) when the PMN–0.33PT SC in the composite is replaced with the KNNTL:Mn SC, a component with a lower piezoelectric activity. This is due to the anisotropy of the elastic properties of the 0–3 FC/polymer matrix (Table 2.4). We remind the reader that, as with the

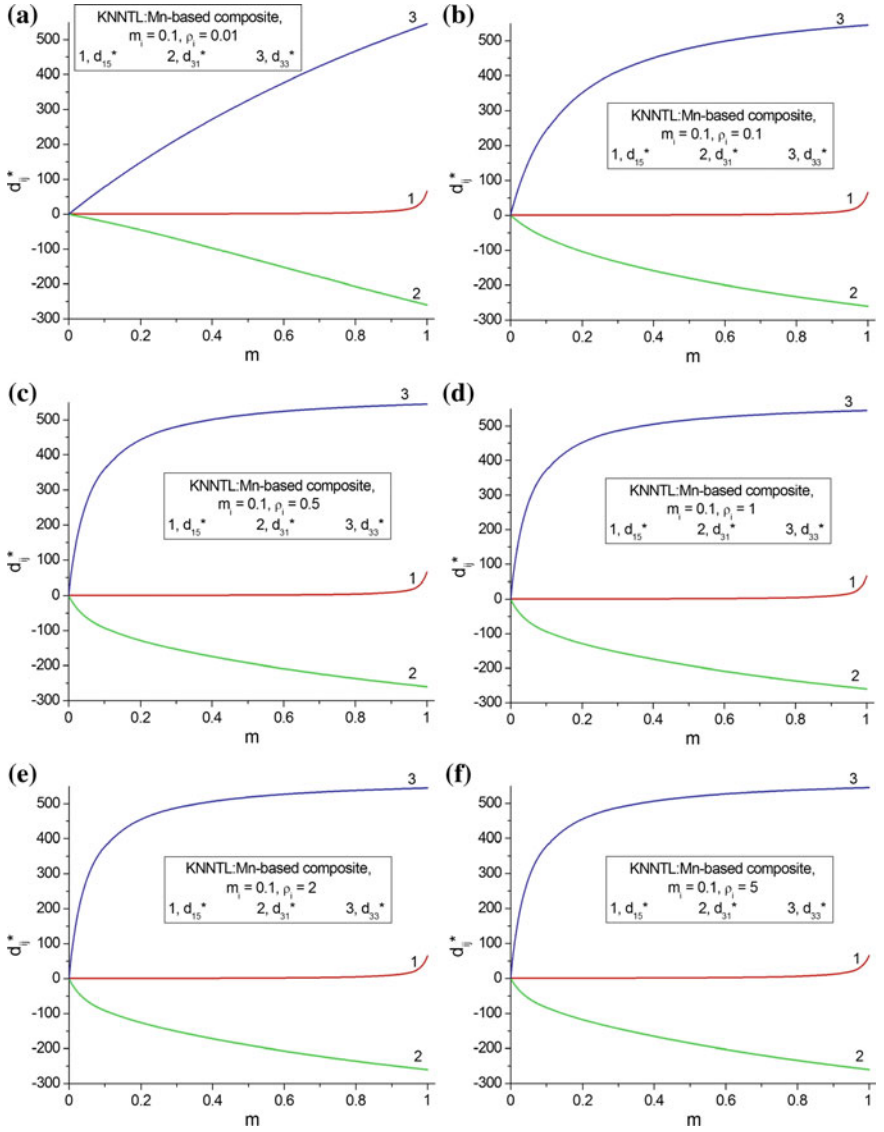

Fig. 2.23 Volume-fraction dependences of piezoelectric coefficients d_{ij}^* (in pC/N) of the 1–0–3 [001]-poled KNNTL:Mn SC/modified $PbTiO_3$ (I) FC/monolithic PE composite with square cross section rods at the volume fraction of FC $m_i = 0.1$. The schematic of the composite is shown in Fig. 2.21

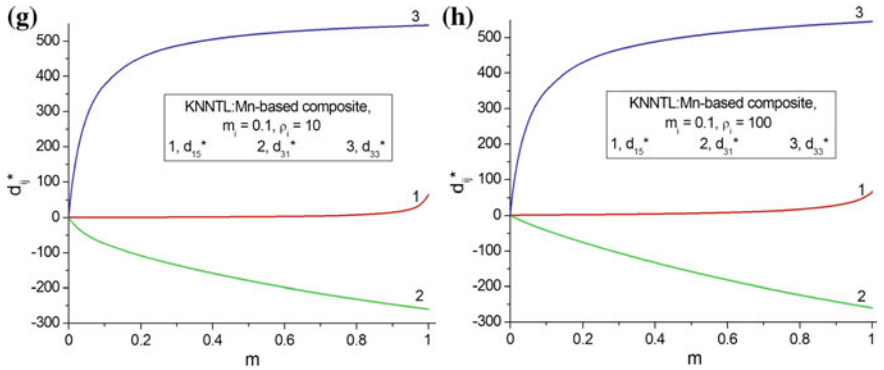

Fig. 2.23 (continued)

[001]-poled PMN–0.33PT SC, the [001]-poled KNNTL:Mn SC is characterised by a relatively small anisotropy of $d_{3j}^{(1)}$, see data in Table 1.2.

When predicting the piezoelectric properties of the KNNTL:Mn-based composite (Fig. 2.23), we also assume that the 0–3 matrix is unpoled. The highly oblate FC inclusions ($\rho_i \gg 1$) in the 0–3 matrix lead to a weakening of the transverse piezoelectric effect from to the SC rods in the composite (Fig. 2.21) and, therefore, lead to a decrease of $|d_{31}^*|$. The system of the SC rods oriented parallel to the poling axis OX_3 favours a strong longitudinal piezoelectric effect, and large values of d_{33}^* are achieved in the presence of FC inclusions at any aspect ratio ρ_I, see curve 3 in Figs. 2.22 and 2.23. This effect due to the 0–3 matrix plays an important role in forming the hydrostatic piezoelectric response of the 1–0–3 composite [46–48] and is to be taken into consideration for the prediction of the PS of related composite structures. The effect of the elastic anisotropy of the 0–3 matrix on the hydrostatic PS of a PZN–0.08PT-based composite leads to large values of its piezoelectric coefficient $d_h^* \sim 10^3$ pC/N [48] while the piezoelectric coefficient $d_h^{(1)}$ of the [001]-poled PZN–0.08PT SC is negative. According to data from Table 1.3, we obtain $d_h^{(1)} = -20$ pC/N.

It can be seen in graphs in Fig. 2.24 that changes in the piezoelectric coefficients d_{ij}^* of the 1–0–3 composite at $\rho_i = 100$ remain small when we vary the volume fraction of FC m_i. This behaviour correlates with minor changes in the ratios of the elastic compliances $s_{11}^{(0-3)}/s_{uv}^{(0-3)}$ of the 0–3 matrix, see data in Table 2.4. On increasing the volume fraction m_i, we observe a decrease of both $|d_{31}^*|$ and d_{33}^*, see Fig. 2.24a, b. In the same case, the piezoelectric coefficient d_{15}^* increases (Fig. 2.24c), but within a restricted range.

Thus, the 1–0–3 SC/FC/polymer composite represents an example of a material wherein three components with contrasting properties influence the PS, and the piezoelectric anisotropy of the composite depends on properties of the 0–3 FC/polymer matrix. The performance of the studied composite is to be taken into account in sensor, actuator and hydroacoustic applications.

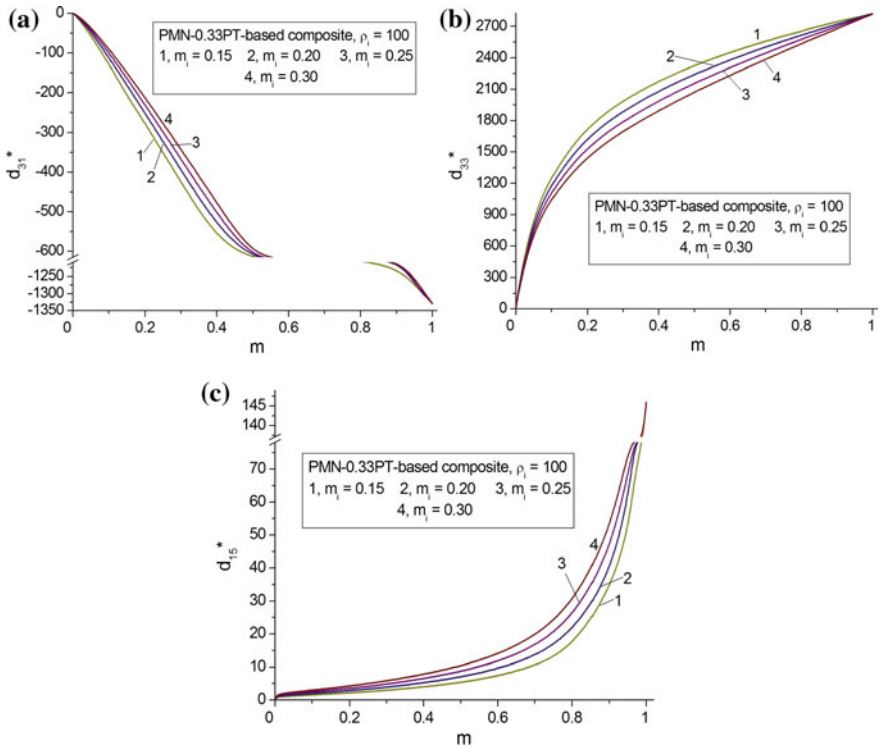

Fig. 2.24 Volume-fraction dependences of piezoelectric coefficients d_{ij}^* (in pC/N) of the 1–0–3 [001]-poled PMN–0.33PT SC/modified $PbTiO_3$ (I) FC/monolithic PE composite with square cross section rods at $\rho_i = 100$. The schematic of the composite is shown in Fig. 2.21

2.3 1–1-Type Composites

A 1–1 connectivity pattern means that each component of a two-component composite is distributed continuously in one direction. Despite the relatively simple microgeometry of the 1–1 composite (Fig. 2.25a) that resembles the well-known 1–3 composite shown in Fig. 2.11, electromechanical properties and related parameters of the 1–1 composite were studied only for some FC/polymer combinations [57, 58]. In Sect. 2.3 we consider examples of the volume-fraction behaviour of the piezoelectric coefficients d_{ij}^* and PS of the 1–1-type FC-based composites.

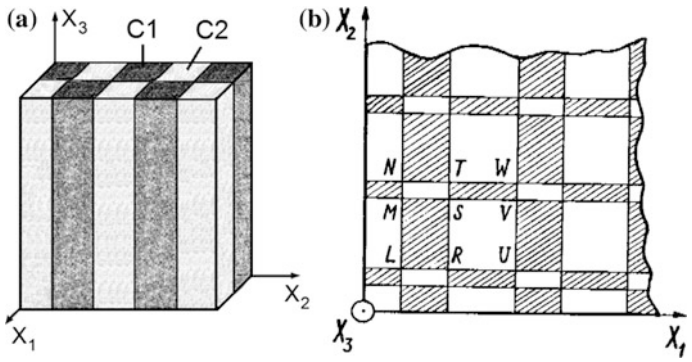

Fig. 2.25 Schematic of the 1–1 composite (**a**) and cross section of the 1–1 composite by the (X_1OX_2) plane (**b**). m and $1 - m$ are volume fractions of components C1 (dashed in **b**) and C2, respectively. ($X_1X_2X_3$) is the rectangular co-ordinate system (**b** reprinted from paper by Glushanin and Topolov [57], with permission from IOP Publishing)

2.3.1 1–1 Ceramic/Polymer Composites

It is assumed that the 1–1 composite contains rectangular FC and polymer parallelepipeds which are alternating in the OX_1 and OX_2 directions (Fig. 2.25). The height of each parallelepiped equals h (that measured along the poling axis OX_3), and conditions $h \gg |LN|$ and $h \gg |LU|$ are valid over the whole composite sample (Fig. 2.25) where the regular distribution of the FC and polymer components is observed. Effective electromechanical properties of the 1–1 composite are determined by means of the matrix method [57] and represented as functions of two parameters, $t = |MS|/|MV|$ and $n = |RS|/|RT|$. The volume faction of FC as a main piezoelectric component in this composite (see C1 in Fig. 2.25a) is given by

$$m = nt + (1-n)(1-t) \tag{2.23}$$

As follows from (2.23), $m = 1$ (limiting case) is achieved at either $n = t = 1$ or $n = t = 0$. If $n = 0$ or 1 and $0 < t < 1$, then we obtain the 2–2 parallel-connected FC/polymer composite (see Sect. 2.1.1). The similar 2–2 composite can be also considered at $t = 0$ or 1 and $0 < n < 1$.

The 1–1 FC/polymer composite poled along OX_3 (Fig. 2.25a) is described by *mm*2 symmetry and characterised by a following peculiarity [57, 58]. The effective electromechanical properties evaluated for a pair of parameters (t, n) remain unchanged for parameters ($1 - t$, $1 - n$). For instance, the piezoelectric coefficients d_{ij}^* obey the condition

$$d_{ij}^*(t,n) = d_{ij}^*(1-t, 1-n) \tag{2.24}$$

Equation (2.24) suggests that the analysis of the PS of the composite can be carried out, for example, at $0 < t \leq 0.5$ and $0 < n < 1$. Hereafter we consider the piezoelectric coefficients d_{3j}^* ($j = 1$, 2 and 3) and their anisotropy. As in the 1–3-type composites, the piezoelectric coefficient d_{15}^* in the 1–1-type composites remains relatively small in the wide volume-fraction (m) range. Such a feature is common in the 1–3, 1–1 and related composite structures because of the system of long piezoelectric rods (see C1 in Figs. 2.11 and 2.25a) distributed continuously along one poling axis.

Examples of the $d_{3j}^*(t, n)$ dependence (Fig. 2.26) show that the piezo-passive polymer component plays the important role in forming the PS of the composite and influences the piezoelectric anisotropy. For the araldite-containing composite, a similar monotonic behaviour of $d_{31}^*(t, n)$ and $d_{32}^*(t, n)$ is observed; see Fig. 2.26a, b. In the composite that contains auxetic PE, we observe the sign-variable and non-monotonic behaviour of $d_{31}^*(t, n)$ and $d_{32}^*(t, n)$; see Fig. 2.26d, e. We note that the non-monotonic behaviour in the latter case is observed at $m \ll 1$, i.e., when the volume fraction of the auxetic polymer component is large and this component can influence the transverse PS of the composite to a large extent. It should be reminded that the change in sgn d_{31}^* and sgn d_{32}^* is observed in the presence of the PCR-7M FC that is characterised by the large transverse piezoelectric coefficient $d_{31}^{(1)}$ (see Table 1.5). At the same time, the $d_{33}^*(t, n)$ dependence is similar in both the composites; see Fig. 2.26c, f. This behaviour means that the polymer component plays a passive role in forming the longitudinal PS of the 1–1 composite.

2.3.2 1–1–0 Ceramic/Porous Polymer Composites

A modification of the 1–1 composite structure shown in Fig. 2.25a leads to changes in the PS. Now we assume that the polymer rods of the composite contain a system of spheroidal air pores that are described by (2.18) relative to the axes of the rectangular co-ordinate system ($X_1X_2X_3$). The schematic of the pore is shown in the inset in Fig. 2.19. As in the case of the 1–3–0 composite considered in Sect. 2.2.4, the pores are regularly distributed in the polymer medium and occupy the sites of a simple tetragonal lattice with unit-cell vectors parallel to the OX_k axes. The shape of each pore is characterised by the aspect ratio $\rho_p = a_{1,p}/a_{3,p}$, and this value is constant over the composite sample. The radius or the largest semi-axis of each pore remains considerably less than the length of the side of the square being the intersection of the FC rod by the (X_1OX_2) plane shown in Fig. 2.25a. The FC/porous polymer composite is characterised by 1–1–0 connectivity. The effective electromechanical properties of the 1–1–0 composite are evaluated in two stages [57, 58], and these stages are similar to those described in Sect. 2.2.4.

Graphs in Fig. 2.27 show that the porous polymer influences the piezoelectric coefficients d_{3j}^* ($j = 1$, 2 and 3) and their anisotropy, and this influence depends on the aspect ratio ρ_p. For instance, at $\rho_p = 0.1$ (prolate pores), we see the considerable

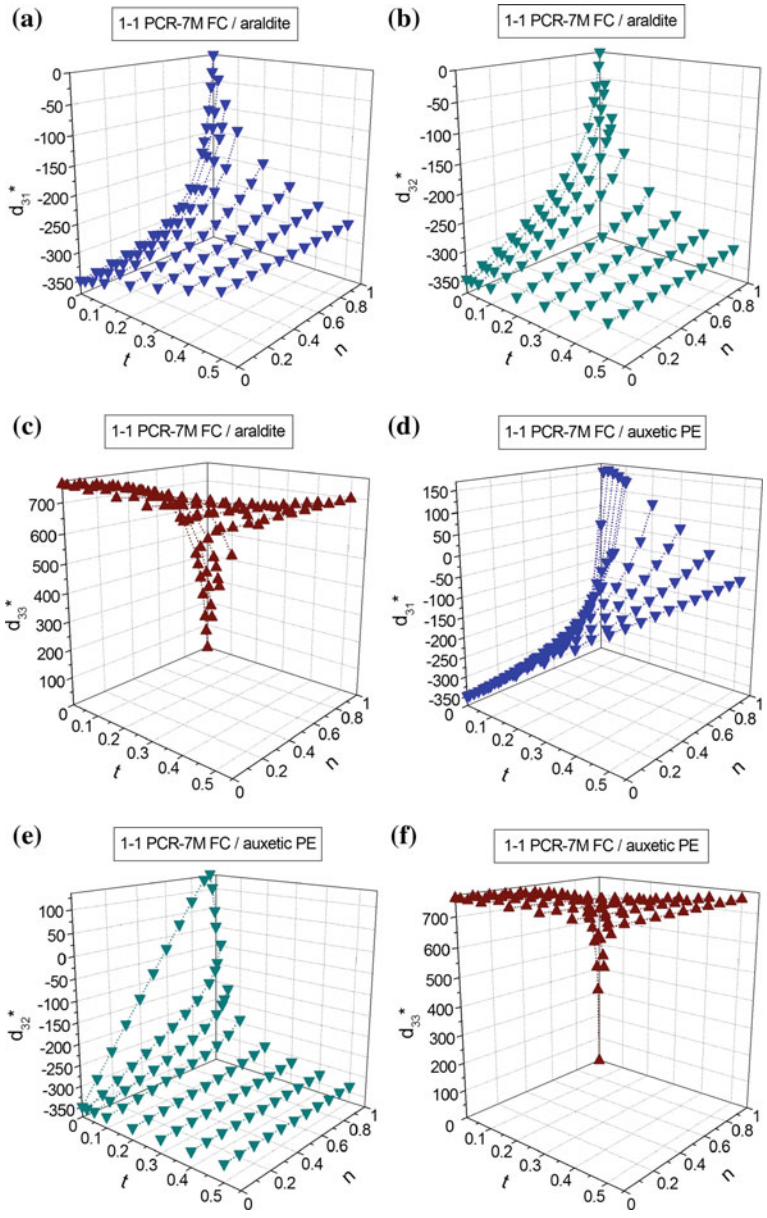

Fig. 2.26 Volume-fraction dependences of piezoelectric coefficients d_{ij}^* (in pC/N) of 1–1 PCR-7M FC/polymer composites. The schematic of the composite is shown in Fig. 2.25a

analogy between the d_{31}^* and d_{32}^* curves shown in Fig. 2.27a, b. At $\rho_p = 1$ (spherical pores), some distinctions between the d_{31}^* and d_{32}^* curves (Fig. 2.27d, e) are observed. At $\rho_p = 100$ (heavily oblate pores), the obvious distinctions between d_{31}^*

and d_{32}^* (Fig. 2.27g, h) are observed. Such an 'evolution' of the curves is concerned with considerable changes in the elastic anisotropy of the porous polymer that influences the transverse PS to a large extent. As for the d_{33}^* curves, they undergo less considerable changes when the aspect ratio ρ_p increases from 0.1 to 100; see Fig. 2.27c, f, i. This is due to the weaker influence of the porous polymer on the longitudinal PS in the studied 1–1–0 composite.

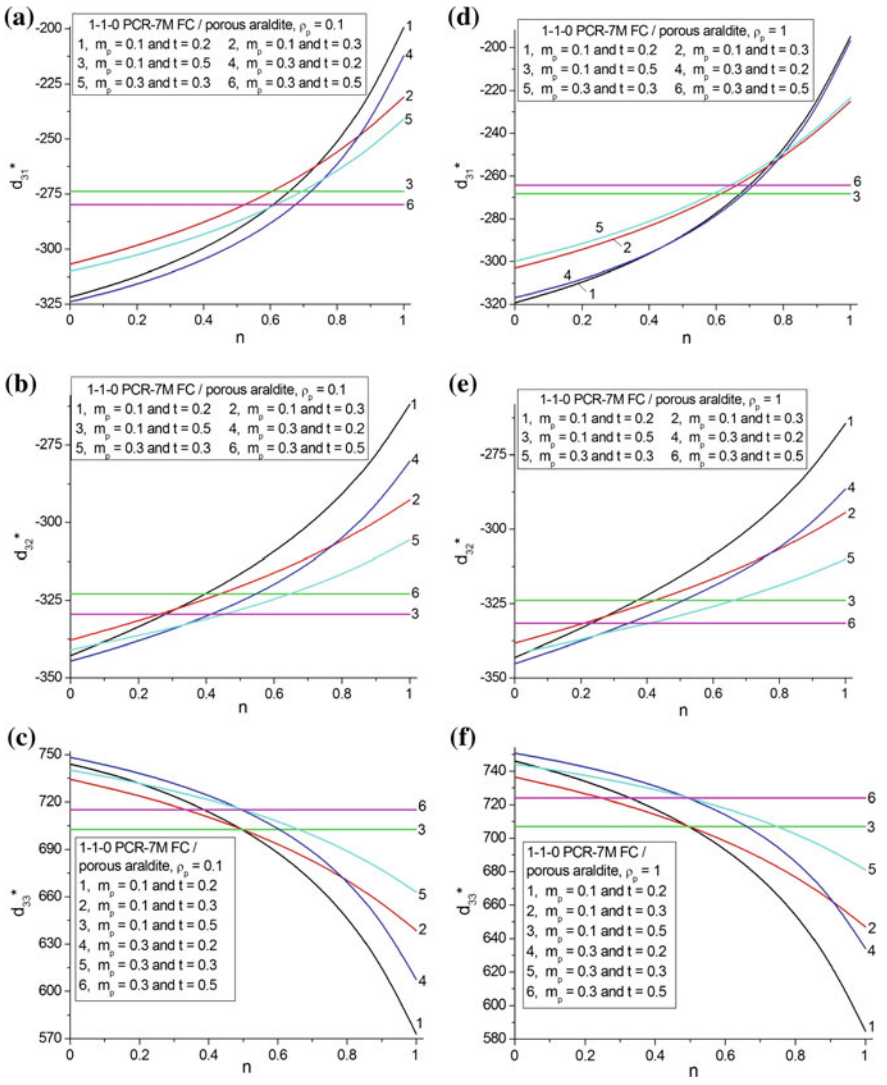

Fig. 2.27 Volume-fraction dependences of piezoelectric coefficients d_{ij}^* (in pC/N) of the 1–1–0 PCR-7M FC/porous araldite composites at ρ_p = 0.1 (**a**–**c**), ρ_p = 1 (**d**–**f**), and ρ_p = 100 (**g**–**i**). The arrangement of the FC rods in the composite is shown in Fig. 2.25a, see C1

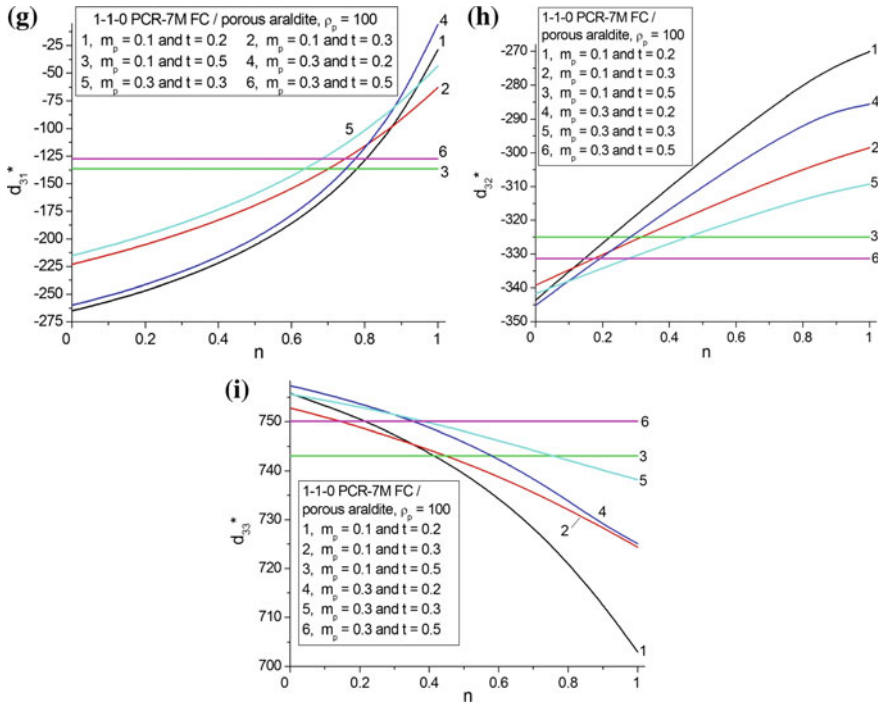

Fig. 2.27 (continued)

Thus, we see an analogy between the PS of the 1–1-type and 1–3-type composites. However the 1–1 composite structure (Fig. 2.25a) opens up additional opportunities to vary the transverse PS and anisotropy of the piezoelectric coefficients d_{3j}^*. This feature of the 1–1-type composites is to be taken into account at a selection of potential materials for piezoelectric transducer, actuator and related applications.

2.4 0–3-Type Composites

The 0–3 composite system is one of the most common piezo-composite types studied earlier (see, for instance, [8, 10–12, 16–18, 59]). The 0–3 composite shown in Fig. 2.28 consists of the three-dimensionally connected matrix reinforced by a system of isolated inclusions. The widespread type of the 0–3 composites is the FC/polymer composite wherein the polymer matrix can be either piezo-passive or piezo-active, and the main piezoelectric component is poled FC [10–12]. Effective electromechanical properties and related parameters of the 0–3 composites are highly dependent on their microstructure, properties and volume fractions of the

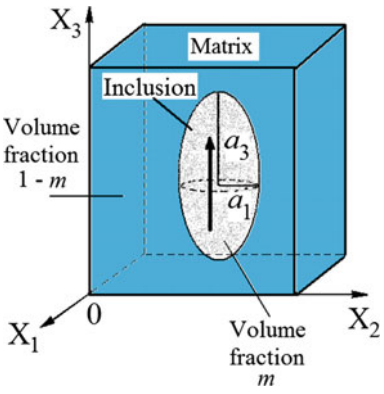

Fig. 2.28 Schematic of the 0–3 composite. The poling direction is denoted by an arrow. a_1 and a_3 are semi-axes of the spheroidal inclusion, m and $1 - m$ are volume fractions of components (reprinted from Topolov et al. [59], with permission from Taylor and Francis)

components, poling conditions, technological factors, etc. [10–14. 59]. In Sect. 2.4 we discuss examples of the PS of various 0–3 composites.

The first example is concerned with a 0–3 ZTS-19 FC/clay composite that was first considered in work [60]. Clay is regarded as a piezo-passive isotropic component with elastic moduli $c_{11} = 4.48 \times 10^8$ Pa and $c_{12} = 1.73 \times 10^8$ Pa and dielectric permittivity $\varepsilon_{pp}/\varepsilon_0 = 8.0$ [61, 62]. ZTS-19 is the typical FC material based on Pb(Zr, Ti)O_3 [10–12], and the full set of electromechanical constants of this FC is given in Table 1.5. It is assumed that the FC inclusions are spheroidal and regularly distributed in the large clay matrix, and the poling axis of each inclusion and the composite sample as a whole is OX_3 (Fig. 2.28). The shape of each FC inclusion is described by (2.13) in the axes of the rectangular co-ordinate system ($X_1X_2X_3$), and the aspect ratio of each inclusion is $\rho = a_1/a_3$. The FC inclusions occupy the sites of a simple tetragonal lattice with unit-cell vectors parallel to the OX_k axes shown in Fig. 2.28. Results of the FEM modelling of the piezoelectric properties of the 0–3 composite are graphically represented in Fig. 2.29. It is seen that even at the ideal poling of the ZTS-19 inclusions aligned in the clay matrix, the piezoelectric coefficients d_{ij}^* of the composite obey the condition

$$d_{ij}^*/d_{ij}^{(1)} \ll 1 \tag{2.25}$$

in the wide volume-fraction (m) range. In Fig. 2.29 we show the volume-fraction dependence of d_{ij}^* in the presence of the non-oblate FC inclusions, i.e., $0 < \rho \leq 1$. The isolated FC (piezoelectric) inclusions surrounded by the piezo-passive matrix promote a lower PS of the 0–3 composite in comparison to the 1–3, 2–2 and 1–1 composites where the piezoelectric component is distributed continuously along the poling axis. For the composite with the oblate FC inclusions ($\rho > 1$), the $d_{ij}^*/d_{ij}^{(1)}$ ratio from (2.25) becomes smaller in comparison to that at $0 < \rho \leq 1$.

In the second example a relatively low PS and validity of (2.25) are predicted for a 0–3 [001]-poled PMN–0.33PT SC/araldite composite (Fig. 2.30). Calculations of d_{ij}^* were performed by means of the FEM. We observe the rapid decrease of $|d_{3j}^*|$

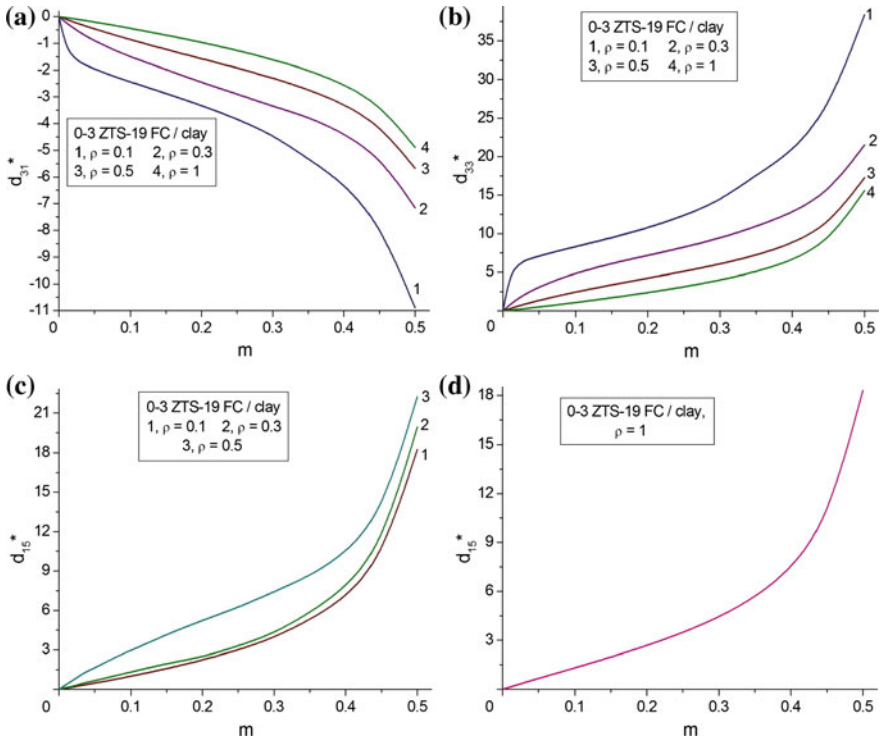

Fig. 2.29 Volume-fraction dependences of piezoelectric coefficients d_{ij}^* (in pC/N) of the 0–3 ZTS-19 FC/clay composite. The schematic of the composite is shown in Fig. 2.28

(Fig. 2.30a, b) on increasing the aspect ratio ρ of the SC inclusions. The piezoelectric coefficient d_{15}^* becomes smaller than that in the 0–3 ZTS-19 FC/clay composite, see Figs. 2.29c, d and 2.30c. Such behaviour may be accounted for by a lesser difference between elastic constants of the SC and polymer components in comparison to the elastic properties of the ZTS-19 FC and clay in the first example. Moreover, the piezoelectric coefficient $d_{15}^{(1)}$ of the ZTS-19 FC is approximately three times larger than $d_{15}^{(1)}$ of the PMN–0.33PT SC; see data in Tables 1.3 and 1.5.

The third example is concerned with a 0–3 SC/FC composite. The piezoelectric performance of such composites was first studied in work [63]. It is assumed that the SC inclusions (volume fraction m) are regularly distributed in the large FC matrix (volume fraction $1 - m$), and both the components are poled along the OX_3 axis (Fig. 2.28). The shape of each SC inclusion is described by (2.13), the aspect ratio is $\rho_i = a_1/a_3$, and a_1, $a_2 = a_1$ and a_3 are semi-axes of the SC inclusion. The domain arrangement in each SC inclusion is shown in Fig. 1.2a, and the co-ordinate axes OX_j obey conditions $OX_1 \| [100]$, $OX_2 \| [010]$ and $OX_3 \| [001]$. Hereby we consider two modes of the arrangement of the SC inclusions, namely, the simple cubic and body-centered arrangements. Among the components of interest, we choose the

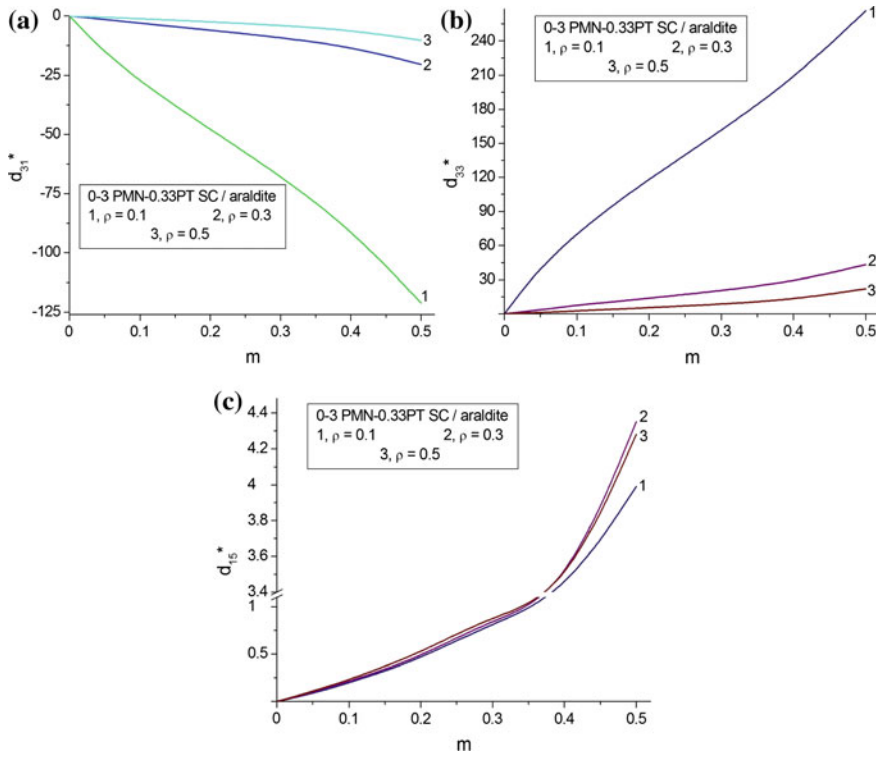

Fig. 2.30 Volume-fraction dependences of piezoelectric coefficients d_{ij}^* (in pC/N) of the 0–3 [001]-poled PMN–0.33PT SC/araldite composite. The schematic of the composite is shown in Fig. 2.28

PMN–0.33PT SC with the high piezoelectric activity (see data in Table 1.3) and the modified $PbTiO_3$ FC with the large piezoelectric anisotropy and moderate piezoelectric activity (see data in Table 1.5). As follows from Table 2.5, changes in the aspect ratio ρ lead to changes in the piezoelectric coefficients d_{ij}^* and piezoelectric anisotropy. At ρ = const and m = const, we observe minor changes in d_{ij}^* when the arrangement of the SC inclusions in the FC matrix changes. We add that the $d_{ij}^*/d_{ij}^{(1)}$ ratio undergoes major changes, however the condition (2.25) holds for the three piezoelectric coefficients of the composite (i.e., for ij = 31, 33 and 15 simultaneously) in restricted ranges of ρ and m.

In the fourth example we assume that the spheroidal SC inclusions are surrounded by the porous polymer medium (see the inset in Fig. 2.19). The polymer matrix contains a system of spheroidal pores with the aspect ratio ρ_p, see also (2.18). As in the case of the 1–3–0 composite, the pores are regularly distributed in the polymer medium and occupy the sites of a simple tetragonal lattice with unit-cell vectors parallel to the OX_k axes (see Sect. 2.2.4). The composite that

Table 2.5 Piezoelectric coefficients d_{ij}^* (in pC/N) and the anisotropy factor $d_{33}^*/|d_{31}^*|$ of the 0–3 [001]-poled PMN–0.33PT SC/modified $PbTiO_3$ FC (I) composite at different modes of the arrangement of SC inclusions, FEM calculations

m	d_{31}^*	d_{33}^*	d_{15}^*	$d_{33}^*/\|d_{31}^*\|$	d_{31}^*	d_{33}^*	d_{15}^*	$d_{33}^*/\| d_{31}^*\|$
	ρ = 0.1, simple cubic arrangement				ρ = 0.1, body-centered arrangement			
0.05	−10.2	64.8	69.4	6.35	−10.3	63.8	69.4	6.39
0.10	−14.2	74.6	70.9	5.25	−14.2	72.8	71.0	5.31
0.20	−23.8	97.5	74.5	4.10	−23.9	93.8	74.6	4.13
0.30	−36.3	126	79.0	3.47	−36.5	120	79.1	3.48
0.50	−75.8	212	92.4	2.80	−77.0	201	92.7	2.80
	ρ = 0.3, simple cubic arrangement				ρ = 0.3, body-centered arrangement			
0.05	−9.99	63.8	69.4	6.39	−10.2	64.2	70.5	6.29
0.10	−13.7	72.8	71.0	5.31	−14.0	73.5	72.9	5.25
0.20	−22.7	93.8	74.6	4.13	−23.4	95.8	77.8	4.09
0.30	−34.5	120	79.1	3.48	−35.8	124	82.6	3.46
0.50	−71.9	201	92.7	2.80	−75.8	212	93.6	2.80
	ρ = 0.5, simple cubic arrangement				ρ = 0.5, body-centered arrangement			
0.05	−9.71	62.9	69.5	6.48	−10.1	63.6	70.6	6.30
0.10	−13.1	70.7	71.0	5.40	−13.8	72.5	72.8	5.25
0.20	−21.3	89.2	74.7	4.19	−22.8	93.5	77.6	4.10
0.30	−31.9	113	79.2	3.54	−34.8	121	82.4	3.48
0.50	−67.6	190	93.1	2.81	−73.9	206	92.5	2.79

consists of the system of the aligned SC inclusions and the porous polymer matrix is described by 0–3–0 connectivity. In the 0–3–0 composite m is the volume fraction of the SC component, and m_p is porosity of the matrix therein. The volume-fraction (m) dependence of the piezoelectric coefficients d_{ij}^* of the 0–3–0 composite with spherical pores (ρ_p = 1) is represented in Fig. 2.31. It is seen that at the aspect ratio of the SC inclusion $\rho > 0.1$, the piezoelectric coefficients $|d_{3j}^*|$ become small, and changes in porosity m_p of the matrix do not lead to appreciable changes in d_{ij}^* of the composite. The piezo-passive polymer matrix and the isolated piezoelectric inclusions promote a weakening of the PS even at the relatively large elastic compliances of the inclusions and matrix in the composite.

2.5 3–β Composites

In the last decades, FC/polymer composites with 3–β connectivity are of interest [10, 16–19, 64] due to their considerable PS and large hydrostatic parameters. The first index 3 means that the first component (FC) is distributed continuously in the composite sample along three co-ordinate axes, and the second index is β = 0, 1, 2, or 3, i.e., the number of the axes, along which the second component (polymer) is

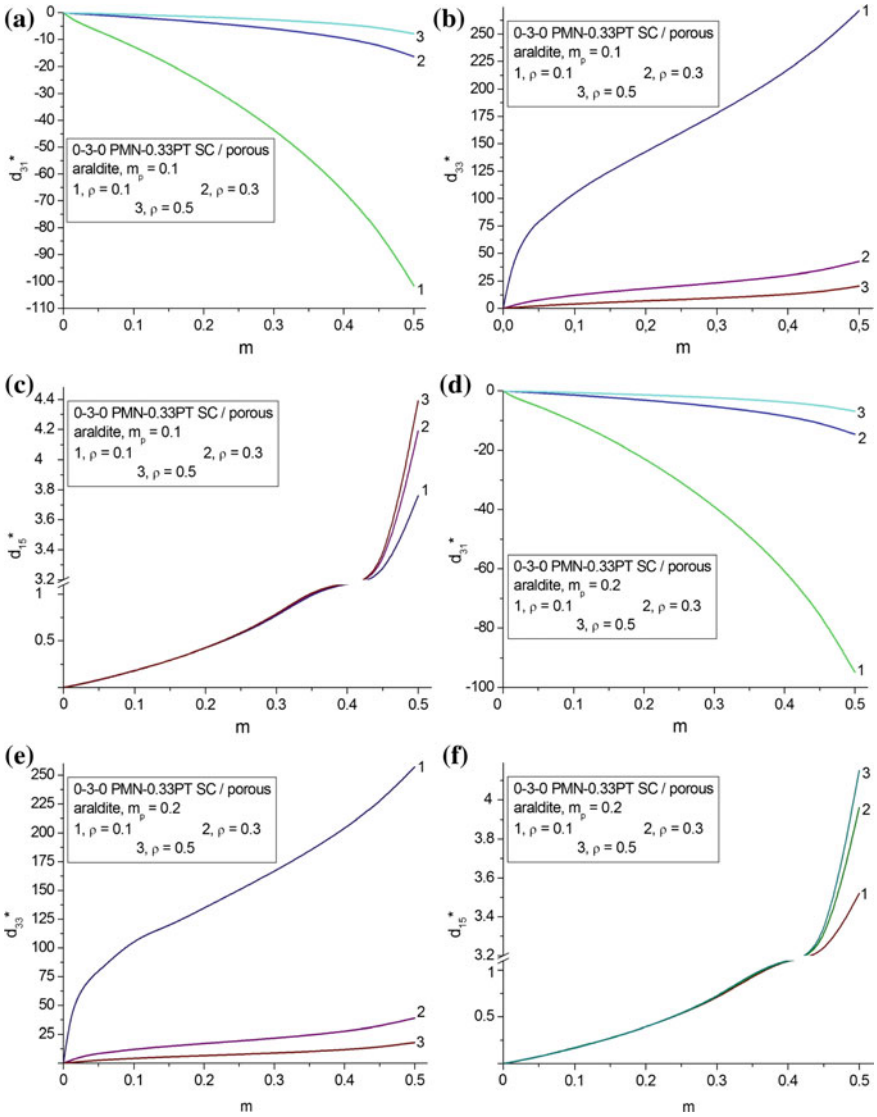

Fig. 2.31 Volume-fraction dependences of piezoelectric coefficients d_{ij}^* (in pC/N) of the 0–3–0 [001]-poled PMN–0.33PT SC/porous araldite composite at porosity of the polymer matrix $m_p = 0.1$ (**a**–**c**) and $m_p = 0.2$ (**d**–**f**). Each pore in the polymer matrix is characterised by the aspect ratio $\rho_p = 1$

distributed, varies from zero to three. To the date, no paper is known where the four connectivity patterns at $\beta = 0$, 1, 2, and 3 are compared and the effective parameters of the 3–β composites are analysed in detail. In Sect. 2.5 we show examples of the piezoelectric properties and their anisotropy in some 3–β composites based on FCs.

Piezoelectric properties of ZTS-19 FC/clay composites with connectivity patterns 3–0 and 3–1 are characterised by similar volume-fraction dependences (Fig. 2.32), and quantitative differences stem from the specifics of the shape of the clay inclusions. The structure of the 3–0 composite is similar to that shown in Fig. 2.28. In the 3–0 composite, the FC matrix contains spheroidal clay inclusions that are distributed over the sample. The shape of each clay inclusion is described by (2.13) in the axes of the rectangular co-ordinate system ($X_1X_2X_3$), and the aspect ratio of each inclusion is $\rho = a_1/a_3$. The clay inclusions occupy the sites of a simple tetragonal lattice with unit-cell vectors parallel to the OX_k axes shown in Fig. 2.28. In the studied 3–0 composite, m_{cl} is the volume fraction of clay, and $1 - m_{cl}$ is the volume fraction of FC. The poling direction of the FC component and composite as a whole is OX_3. The 3–1 composite is regarded as a limiting case of the 3–0 composite at $\rho = 0$. In the 3–1 composite, the regular arrangement of clay circular rods is also assumed.

Graphs in Fig. 2.32 were built by taking into account FEM calculations. It is seen that the transverse piezoelectric effect becomes stronger (Fig. 2.32a) on increasing the aspect ratio ρ, i.e., at the transition from the prolate to spherical shape

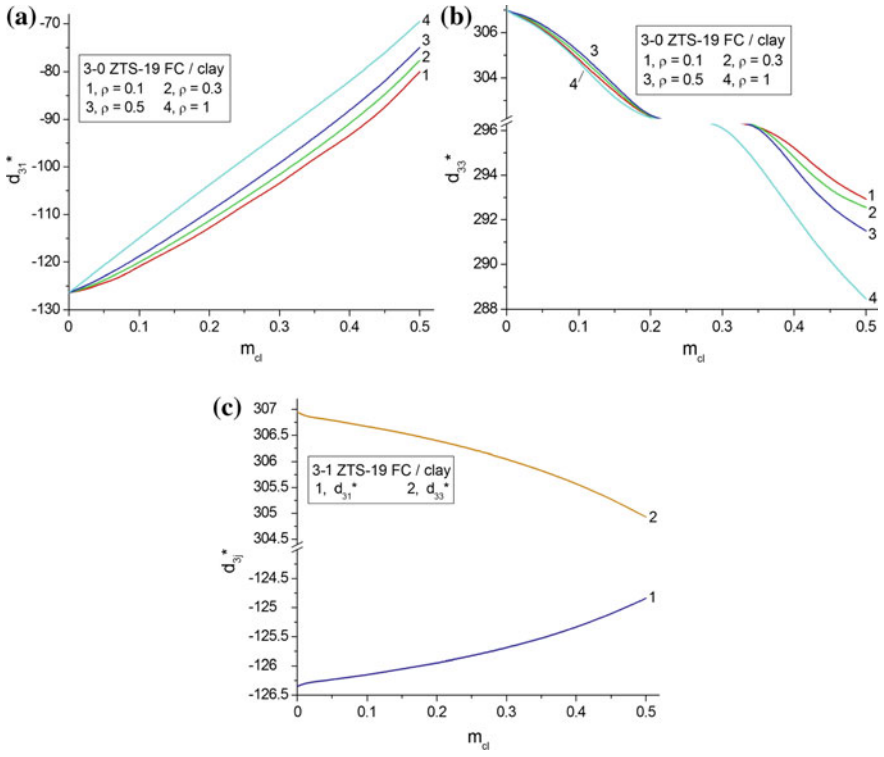

Fig. 2.32 Volume-fraction dependences of piezoelectric coefficients d_{3j}^* (in pC/N) of 3–0 (**a**–**b**) and 3–1 (**c**) ZTS-19 FC/clay composites

of the clay inclusion. The weakening of the longitudinal piezoelectric effect on increasing the aspect ratio ρ (Fig. 2.32b) is caused by the shape of the same clay inclusions.

For instance, the larger piezoelectric coefficient d_{33}^* at m_{cl} = const is expected in the presence of the clay inclusions with a smaller aspect ratio ρ. Minor changes in the d_{33}^* curves at $0 < \rho \leq 1$ (Fig. 2.32b) are accounted for by the strong influence of the poled FC matrix on the PS of the composite. Figure 2.32c shows that changes in d_{3j}^* of the 3–1 composite are observed in the narrower ranges in comparison to the 3–0 composite. Such a feature is concerned with the presence of the clay inclusions that are continuously distributed along the poling axis OX_3 and make no serious obstacles at the poling of the composite sample at the electric field $\boldsymbol{E} \| OX_3$. It should be added that the results on the FEM modelling of the electromechanical properties of the 3–0 composite were used in work [60] where the ZTS-19 FC/clay composite was first manufactured and characterised as a piezo-active composite with a few connectivity patterns.

Examples of the volume-fraction behaviour of the piezoelectric coefficient d_{33}^* of composites based on the PZT-5H FC are shown in Fig. 2.33, where m is the volume fraction of the FC component. The related 3–β composites with the regular arrangement of their components were manufactured and studied in work [19]. The largest values of d_{33}^* at m = const are achieved in the 3–1 composite (Fig. 2.33a) where the polymer rods are distributed continuously along the poling axis OX_3. A decrease of d_{33}^* at m = const in the 3–2 and 3–3 composites (Fig. 2.33b, c) in comparison to d_{33}^* of the 3–1 composite is caused by technological factors, non-dense contacts between the FC and polymer components in samples, incomplete poling of some fragments of the samples, etc.

Our analysis of the $d_{33}^*(m)$ dependences in Fig. 2.33 enables us to conclude that these dependences can be approximated by

$$d_{33}^*(m) = a_0 + a_1 m + a_2 m^2 + a_3 m^3. \tag{2.26}$$

In (2.26) a_i are coefficients that do not depend on m. We add for a comparison that a volume-fraction dependence $d_{33}^*(m_{pl})$ in a ZTS-19 FC/polymer composite from work [65] is represented as

$$d_{33}^*\left(m_{pl}\right) = a_0^* + a_1^* m_{pl} + a_2^* {m_{pl}}^2 + a_3^* {m_{pl}}^3 + a_4^* {m_{pl}}^4 \tag{2.27}$$

In (2.27) a_i* are coefficients that do not depend on m_{pl}, and m_{pl} is the volume fraction of the polymer component. A difference between the polynomials (2.26) and (2.27) can be accounted for by specifics of the composite mcirogeometry, poling conditions and other factors.

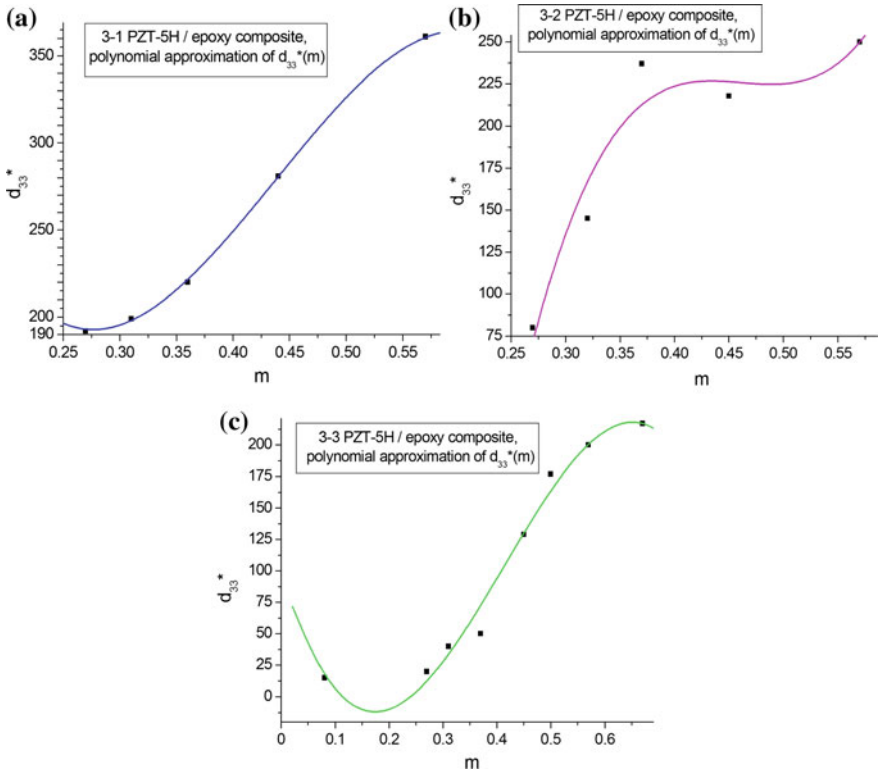

Fig. 2.33 Volume-fraction dependences of the piezoelectric coefficient d_{33}^* (in pC/N) of 3–β PZT-5H FC/epoxy composites and examples of the polynomial approximation of $d_{33}^*(m)$ at $\beta = 1$ (**a**), $\beta = 2$ (**b**) and $\beta = 3$ (**c**). Experimental points (black squares in graphs) are adapted from work [19])

2.6 Electromechanical Coupling Factors and Their Relations to d_{ij}^*

Based on (1.16)–(1.18), we analyse ECFs related to the 1–3 SC/polymer composite. Figure 2.34a shows links between the piezoelectric coefficient d_{31}^* and ECFs k_{31}^* and k_p^* which are concerned with the transverse piezoelectric effect. In Fig. 2.34b links between the piezoelectric coefficient d_{33}^* and ECFs k_{33}^* and k_t^* are observed, and these parameters are concerned with the longitudinal piezoelectric effect. The effective parameters of the 1–3 PMN-0.33PT-based composite were evaluated by means of the matrix method, see Sect. 2.2.2. A correlation between $d_{3j}^*(m)$ and $k_{3j}^*(m)$ (see curves 1 and 2 in Fig. 2.34) is accounted for by a restricted influence of the dielectric and elastic properties of the 1–3 composite on its electromechanical coupling and by the proportionality $k_{3j}^* \sim d_{3j}^*$ in accordance with (1.16). A small

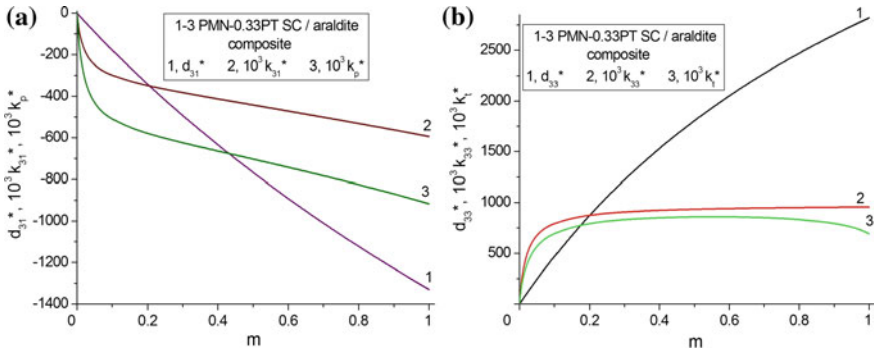

Fig. 2.34 Volume-fraction (m) dependence of piezoelectric coefficients d_{3j}^* (in pC/N) and ECFs k_{3j}^*, k_p^* and k_t^* in the 1–3 [001]-poled PMN–0.33PT SC/araldite composite. The schematic of the composite is shown in Fig. 2.11

difference between the ECFs k_{33}^* and k_t^* (see curves 2 and 3 in Fig. 2.34b) in the wide m range is typical of the 1–3 composite poled along the OX_3 axis [12, 42, 44].

A considerable anisotropy of the ECFs can be observed in the 1–3-type composite wherein the matrix is characterised by a specific elastic anisotropy [55]. This elastic anisotropy is caused by auxetic polymers, pores or FC inclusions in the polymer medium [8, 46–48, 52, 54, 55]. Examples of the large anisotropy of the piezoelectric coefficients d_{3j}^* and ECFs related to the longitudinal and transverse piezoelectric effects in the 1–3–0 composite with the porous polymer matrix are shown in Table 2.6. The highly oblate pores promote the larger anisotropy of d_{3j}^* on increasing porosity m_p in the polymer matrix. The similar conditions for the large anisotropy of the ECFs are valid in narrower volume-fraction ranges $[m_1, m_2]$ in comparison to the anisotropy of d_{3j}^*, see 3rd, 4th and 5th columns in Table 2.6. On increasing porosity m_p in the matrix, the volume-fraction range corresponding to the

Table 2.6 Volume-fraction ranges $[m_1, m_2]$ wherein conditions for the large anisotropy of piezoelectric coefficients d_{3j}^* and ECFs hold for the 1–3–0 [001]-poled PMN–0.33PT SC/porous araldite composite[a]

ρ_p	m_p	Validity of the condition $d_{33}^*/\lvert d_{31}^*\rvert \geq 5$	Validity of the condition $k_{33}^*/\lvert k_{31}^*\rvert \geq 5$	Validity of the condition $k_t^*/\lvert k_p^*\rvert \geq 5$
10	0.2	[0.001, 0.048]	–	–
10	0.3	[0.001, 0.111]	–	–
100	0.1	[0.001, 0.273]	[0.001, 0.196]	–
100	0.2	[0.001, 0.300]	[0.001, 0.245]	[0.001, 0.093]
100	0.3	[0.001, 0.309]	[0.001, 0.275]	[0.001, 0.130]

The schematic of the composite is shown in Fig. 2.19

[a]The volume fraction of SC m is varied from 0.001 to 0.999

large anisotropy of d_{3j}^* becomes wider, see 3rd column in Table 2.6 at ρ_p = 100. This effect is concerned with the influence of elastic properties of the porous polymer matrix on the ECFs of the composite [12, 55], and such an influence strongly depends on the oscillation mode and volume fraction of SC. It should be reminded that the PMN–0.33PT SC, the only piezoelectric component in the studied 1–3–0 composite, does not exhibit the remarkable anisotropy of the piezoelectric coefficients $d_{3j}^{(1)}$, see data in Table 1.3.

2.7 Hydrostatic Piezoelectric Response and Its Relation to d_{ij}^*

As is known from Sect. 1.3, the hydrostatic piezoelectric coefficient d_h is directly used as a measure of PS at the transmitter function of the hydrophone. The effective hydrostatic piezoelectric coefficient d_h^* from (2.1) is related to a composite sample with electrodes applied perpendicular to the OX_3 axis, and this axis is often regarded as a poling axis of the composite [4, 10, 12, 17]. The piezoelectric coefficient d_h^* from (2.21) has important links to the hydrostatic squared figure of merit (2.2) and hydrostatic ECF

$$k_h^* = d_h^* / \left(\varepsilon_{33}^{*\sigma} s_h^{*E}\right)^{1/2} \tag{2.28}$$

In (2.28) $\varepsilon_{33}^{*\sigma}$ is the dielectric permittivity of the composite at σ = const, and

$$s_h^{*E} = \sum_{a=1}^{3} \sum_{b=1}^{3} s_{ab}^{*E} \tag{2.29}$$

is the hydrostatic elastic compliance of the composite at E = const.

An example of interrelations between the hydrostatic parameters from (2.1), (2.2) and (2.28) is shown in Fig. 2.35. Calculations were performed by means of the matrix method. The maximum of each parameter shown in Fig. 2.35 is caused by the behaviour of the piezoelectric coefficients d_{3j}^* shown in Fig. 2.16a, see curves 2 and 3. Maxima of $(Q_h^*)^2$ from (2.2) and k_h^* from (2.28) are observed at smaller volume fractions m (curves 2 and 3 in Fig. 2.35) in comparison to max d_h^* (curve 1 in Fig. 2.35). This is accounted for by the influence of dielectric properties of the composite on $(Q_h^*)^2$ and k_h^*. The diffuse min k_h^* at $m \approx 0.9$ (curve 2 in Fig. 2.35) is caused by the non-monotonic volume-fraction behaviour of elastic compliances s_{ab}^{*E} that determine s_h^{*E} from (2.29).

In the related 1–3–0 composite, maxima of the hydrostatic parameters from (2.1), (2.2) and (2.28) depend on the aspect ratio of the air pore ρ_p and porosity m_p which are characteristics of the matrix, see Fig. 2.19. Table 2.7 suggests that increasing maxima of the parameters correlates with increasing the aspect ratio ρ_p at

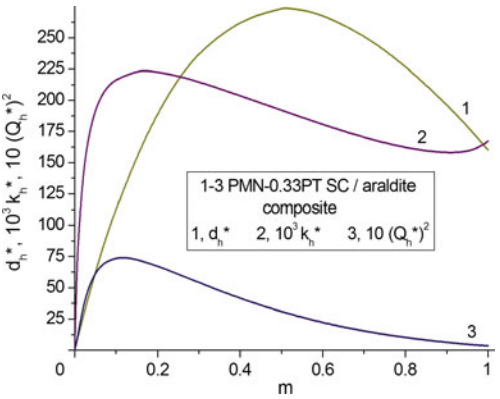

Fig. 2.35 Volume fraction dependence of the hydrostatic piezoelectric coefficient d_h^* (in pC/N), squared figure of merit $(Q_h^*)^2$ (in 10^{-12} Pa^{-1}) and ECF k_h^* of the 1–3 [001]-poled PMN–0.33PT SC/araldite composite. The schematic of the composite is shown in Fig. 2.11

Table 2.7 Maximum values of the hydrostatic piezoelectric coefficient d_h^* (in pC/N), squared figure of merit $(Q_h^*)^2$ (in 10^{-12} Pa^{-1}) and ECF k_h^* of the 1–3–0 [001]-poled PMN–0.33PT SC/porous araldite composite

ρ_p	Max d_h^*	Max $[(Q_h^*)^2]$	Max k_h^*
Composite at $m_p = 0.1$			
0.1	282 ($m = 0.486$)[a]	8.32 ($m = 0.105$)	0.196 ($m = 0.150$)
0.5	294 ($m = 0.478$)	9.19 ($m = 0.109$)	0.219 ($m = 0.145$)
1	313 ($m = 0.464$)	10.8 ($m = 0.099$)	0.240 ($m = 0.138$)
10	609 ($m = 0.356$)	56.8 ($m = 0.066$)	0.448 ($m = 0.096$)
100	1390 ($m = 0.194$)	684 ($m = 0.020$)	0.760 ($m = 0.046$)
Composite at $m_p = 0.2$			
0.1	291 ($m = 0.463$)	9.43 ($m = 0.096$)	0.177 ($m = 0.134$)
0.5	316 ($m = 0.448$)	11.4 ($m = 0.091$)	0.214 ($m = 0.125$)
1	353 ($m = 0.425$)	15.1 ($m = 0.084$)	0.254 ($m = 0.114$)
10	829 ($m = 0.294$)	133 ($m = 0.045$)	0.549 ($m = 0.070$)
100	1640 ($m = 0.146$)	1520 ($m = 0.011$)	0.816 ($m = 0.032$)
Composite at $m_p = 0.3$			
0.1	303 ($m = 0.438$)	10.9 ($m = 0.086$)	0.162 ($m = 0.117$)
0.5	340 ($m = 0.418$)	14.2 ($m = 0.079$)	0.211 ($m = 0.106$)
1	394 ($m = 0.390$)	20.8 ($m = 0.071$)	0.265 ($m = 0.094$)
10	998 ($m = 0.252$)	236 ($m = 0.032$)	0.609 ($m = 0.054$)
100	1780 ($m = 0.120$)	2550 ($m = 0.007$)	0.840 ($m = 0.024$)

The schematic of the composite is shown in Fig. 2.19

[a]The volume fraction of SC which is related to the maximum of the hydrostatic parameter is given in parentheses

m_p = const. This is consistent with data in Table 2.6 and with the statement that the elastic anisotropy of the porous polymer matrix strongly influences the hydrostatic parameters of the 1–3–0 composite.

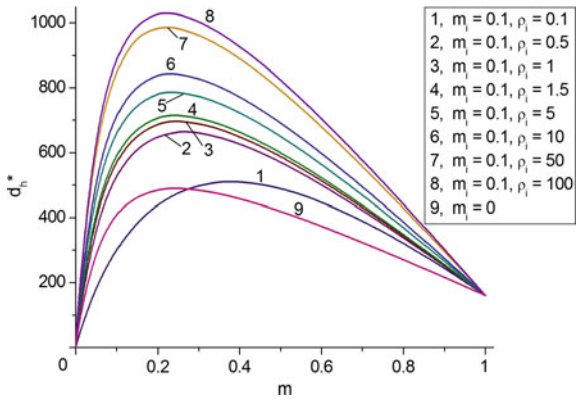

Fig. 2.36 Volume-fraction dependence of the hydrostatic piezoelectric coefficient d_h^* (in pC/N) of the 2–0–2 [001]-poled PMN–0.33PT SC/modified $PbTiO_3$ FC (I)/PE composite. Curve 9 is related to the 2–2 [001]-poled PMN–0.33PT SC/PE composite (reprinted from paper by Topolov et al. [39], with permission from Taylor and Francis)

The similar behaviour of the hydrostatic parameters from (2.1), (2.2) and (2.28) is observed in the 2–0–2 SC/FC/polymer composite described in Sect. 2.1.3. Changes in the aspect ratio of the FC inclusions ρ_i in the 0–3 FC/polymer layer lead to changes in the piezoelectric properties and their anisotropy (Fig. 2.9). As a result, the larger hydrostatic piezoelectric coefficient d_h^* of the 2–0–2 composite is achieved at the larger aspect ratio ρ_i (Fig. 2.36). We note that the max d_h^* value at ρ_i = 100 (curve 8 in Fig. 2.36) is approximately two times larger than the max d_h^* value related to the 2–2 composite (curve 9 in Fig. 2.36) that does not contain the FC inclusions. Such a large difference is achieved even at the relatively small volume fraction of FC m_i = 0.1. The reason for the large difference is concerned [39] with the large elastic anisotropy of the 0–3 FC/polymer layer at $\rho_i \gg 1$, and this effect is to be taken into account at predicting the effective properties and hydrostatic parameters of advanced piezo-active composites.

2.8 Conclusion

This chapter has been devoted to the piezoelectric coefficients d_{ij}^*, their anisotropy and links between microgeometric characteristics of piezo-active composites and their d_{ij}^*. The piezoelectric coefficients d_{ij}^* play the important role at the analysis of the PS and ways for improving the performance and PS of the composites. The main results of this chapter are formulated as follows.

(i) Examples of the PS of the composites are considered for the following connectivity patterns: 0–3, 0–3–0, 1–1, 1–1–0, 1–3, 1–2–2, 1–0–3, 1–3–0, 2–2, 2–0–2, 3–0, 3–1, 3–2, and 3–3. The studied composites are based on either FCs or domain-engineered SCs. Changes in the volume fraction of the piezoelectric component and microgeometry of the composite enable us to vary d_{ij}^* and their anisotropy in wide ranges. As follows from the analysis

of the volume-fraction dependences of d_{ij}^*, the main emphasis at the study of the microgeometry–PS relations is to be placed on the longitudinal and transverse piezoelectric coefficients d_{ij}^* and ways to control the PS for the specific connectivity pattern.

(ii) The system of the aligned FC (or SC) rods in the large polymer matrix promotes the large piezoelectric coefficient d_{33}^* and related ECFs.

(iii) The auxetic polymer matrix strongly influences the elastic and piezoelectric anisotropy of the composite and the anisotropy of its ECFs due to the negative Poisson's ratio of the polymer. Volume fractions that correspond to $d_{31}^* = 0$ depend on the elastic properties of the FC (or SC) and polymer components.

(iv) The system of oblate spheroidal air pores in the polymer matrix promotes the considerable anisotropy of the piezoelectric coefficients d_{ij}^* and ECFs, and this trend is often observed in the 1–3-type and 2–2-type composites. The elastic anisotropy of the composite plays the important role in the formation of the large anisotropy of the ECFs. The large hydrostatic parameters are achieved in the same composites with the porous polymer matrix.

(v) In the 2–0–2 composite with contrasting properties of the components, the SC component strongly influences the PS. The 0–3 FC/polymer layer exhibits a considerable level of elastic anisotropy and plays the important role in forming the large piezoelectric anisotropy and pronounced hydrostatic piezoelectric response of the 2–0–2 composite.

(vi) Links between the PS, ECFs and hydrostatic parameters of the 1–3-type composites are important at the prediction of their performance and at the selection of materials for piezotechnical applications. In the 1–0–3 SC/FC/polymer composite with contrasting properties of components, the 0–3 matrix influences the piezoelectric anisotropy of the composite.

(vii) In the 0–3 composite the PS and piezoelectric anisotropy can be varied in restricted ranges because of the isolated piezoelectric inclusions. The porous matrix with 3–0 connectivity can influence the piezoelectric anisotropy of the 0–3–0 composite to some extent.

(viii) The $d_{33}^*(m)$ dependence (2.26) related to the 3–β FC/polymer composites (β = 1, 2 and 3) suggests that their longitudinal PS is mainly caused by the continuous distribution of the FC component along three co-ordinate axes and depends on the connectivity index β to a small degree.

Data from this chapter can be taken into account to predict the PS, electromechanical coupling and hydrostatic piezoelectric response of various two- and three-component composites. These materials can be of interest in modern piezotechnical applications including transducers, sensors, actuators, hydrophones, and energy-harvesting systems where the piezoelectric coefficients d_{ij}^* and related parameters are exploited.

References

1. Ikeda T (1990) Fundamentals of piezoelectricity. Oxford University Press, Oxford, New York, Toronto
2. Zheludev IS (1971) Physics of crystalline dielectrics. Vol 2: Electrical properties. Plenum, New York
3. Jaffe B, Cook WR, Jaffe H (1971) Piezoelectric ceramics. Academic Press, London, New York
4. Sherman CH, Butler JL (2007) Transducers and arrays for underwater sound. Springer, New York
5. Tichý J, Erhart J, Kittinger E, Přívratská J (2010) Fundamentals of piezoelectric sensorics. Mechanical, dielectric, and thermodynamical properties of piezoelectric materials. Springer, Berlin
6. Uchino K (2008) Piezoelectric motors and transformers. In: Heywang W, Lubitz K, Wersing W (eds) Piezoelectricity, evolution and future of a technology. Springer, Berlin, pp 257–277
7. Haertling G (1999) Ferroelectric ceramics: history and technology. J Am Ceram Soc 82:797–818
8. Bowen CR, Topolov VYu, Kim HA (2016) Modern piezoelectric energy-harvesting materials. Springer International Publishing, Switzerland
9. Shvarstman VV, Kholkin AL (2011) Nanoscale investigation of polycrystalline ferroelectric materials via piezoresponse force microscopy. In: Pardo L, Ricote J (eds) Multifunctional polycrystalline ferroelectric materials. Processing and properties. Springer, Dordrecht, pp 409–468
10. Topolov VYu, Bowen CR (2009) Electromechanical properties in composites based on ferroelectrics. Springer, London
11. Khoroshun LP, Maslov BP, Leshchenko PV (1989) Prediction of effective properties of piezo-active composite materials. Naukova Dumka, Kiev (in Russian)
12. Topolov VYu, Bisegna P, Bowen CR (2014) Piezo-active composites. Orientation effects and anisotropy factors. Springer, Berlin, Heidelberg
13. Chan HLW, Ng PKL, Choy CL (1999) Effect of poling procedure on the properties of lead zirconate titanate/vinylidene fluoride-trifluoroethylene composites. Appl Phys Lett 74:3029–3031
14. Nan CW, Weng GJ (2000) Influence of polarization orientation on the effective properties of piezoelectric composites. J Appl Phys 88:416–423
15. Newnham RE, Skinner DP, Cross LE (1978) Connectivity and piezoelectric-pyroelectric composites. Mater Res Bull 13:525–536
16. Gururaja TR, Safari A, Newnham RE, Cross LE (1988) Piezoelectric ceramic-polymer composites for transducer applications. In: Levinson LM (ed) Electronic ceramics: properties, devices, and applications. Marcel Dekker, New York, pp 92–128
17. Akdogan EK, Allahverdi M, Safari A (2005) Piezoelectric composites for sensor and actuator applications. IEEE Trans Ultrason Ferroelectr Freq Control 52:746–775
18. Safari A, Akdogan EK (2006) Rapid prototyping of novel piezoelectric composites. Ferroelectrics 331:153–179
19. Smay JE, Tuttle B, Cesarano J III (2008) Robocasting of three-dimensional piezoelectric structures. In: Safari A, Akdoğan EK (eds) Piezoelectric and acoustic materials for transducer applications. Springer, New York, pp 305–318
20. Topolov VYu, Turik AV (2000) Non-monotonic concentration dependence of electromechanical properties of piezo-active 2–2 composites. J Phys D Appl Phys 33:725–737
21. Grekov AA, Kramarov SO, Kuprienko AA (1987) Anomalous behavior of the two-phase lamellar piezoelectric texture. Ferroelectrics 76:43–48
22. Levassort F, Lethiecq M, Millar C, Pourcelot L (1998) Modeling of highly loaded 0–3 piezoelectric composites using a matrix method. IEEE Trans Ultrason Ferroelectr Freq Control 45:1497–1505
23. Gibiansky LV, Torquato S (1997) On the use of homogenization theory to design optimal piezocomposites for hydrophone applications. J Mech Phys Solids 45:689–708

24. Grekov AA, Kramarov SO, Kuprienko AA (1989) Effective properties of a transversely isotropic piezoelectric composite with cylindrical inclusions. Mech Compos Mater 25:54–61
25. Evans KE, Alderson KL (1992) The static and dynamic moduli of auxetic microporous polyethylene. J Mater Sci Lett 11:1721–1724
26. Ren K, Liu Y, Geng X, Hofmann HF, Zhang QM (2006) Single crystal PMN–PT/epoxy 1–3 composite for energy-harvesting application. IEEE Trans Ultrason Ferroelectr Freq Control 53:631–638
27. Wang F, He C, Tang Y (2007) Single crystal $0.7Pb(Mg_{1/3}Nb_{2/3})O_3$–$0.3PbTiO_3$/epoxy 1–3 piezoelectric composites prepared by the lamination technique. Mater Chem Phys 105:273–277
28. Topolov VYu, Krivoruchko AV (2009) Polarization orientation effect and combination of electromechanical properties in advanced $0.67Pb(Mg_{1/3}Nb_{2/3})O_3$–$0.33PbTiO_3$ single crystal/polymer composites with 2–2 connectivity. Smart Mater Struct 18:011–065
29. Zhang R, Jiang B, Cao W (2001) Elastic, piezoelectric, and dielectric properties of multidomain $0.67Pb(Mg_{1/3}Nb_{2/3})O_3$–$0.33PbTiO_3$ single crystals. J Appl Phys 90:3471–3475
30. Zhang R, Jiang B, Cao W (2003) Single-domain properties of $0.67Pb(Mg_{1/3}Nb_{2/3})O_3$–$0.33PbTiO_3$ single crystals under electric field bias. Appl Phys Lett 82:787–789
31. Peng J, Luo H, He T, Xu H, Lin D (2005) Elastic, dielectric, and piezoelectric characterization of $0.70Pb(Mg_{1/3}Nb_{2/3})O_3$–$0.30PbTiO_3$ single crystal. Mater Lett 59:640–643
32. Liu G, Jiang W, Zhu J, Cao W (2011) Electromechanical properties and anisotropy of single- and multi-domain $0.72Pb(Mg_{1/3}Nb_{2/3})O_3$–$0.28PbTiO_3$ single crystals. Appl Phys Lett 99:162901
33. Sun E, Cao W, Jiang W, Han P (2011) Complete set of material properties of single domain $0.24Pb(In_{1/2}Nb_{1/2})O_3$–$0.49Pb(Mg_{1/3}Nb_{2/3})O_3$-$0.27PbTiO_3$ single crystal and the orientation effects. Appl Phys Lett 99:032901
34. Yin J, Jiang B, Cao W (2000) Elastic, piezoelectric, and dielectric properties of $0.955Pb(Zn_{1/3}Nb_{2/3})O_3$–$0.045PbTiO_3$ single crystals. IEEE Trans Ultrason Ferroelectr Freq Control 47:285–291
35. Zhang R, Jiang B, Cao W, Amin A (2002) Complete set of material constants of $0.93Pb(Zn_{1/3}Nb_{2/3})O_3$–$0.07PbTiO_3$ domain engineered single crystal. J Mater Sci Lett 21:1877–1879
36. Zhang S, Li F, Jiang X, Kim J, Luo J, Geng X (2015) Advantages and challenges of relaxor-$PbTiO_3$ ferroelectric crystals for electroacoustic transducers—a review. Prog Mater Sci 68:1–66
37. Turik AV, Topolov VYu (1997) Ferroelectric ceramics with a large piezoelectric anisotropy. J Phys D Appl Phys 30:1541–1549
38. Dongyu X, Xin C, Shifeng H (2015) Investigation of inorganic fillers on properties of 2–2 connectivity cement/polymer based piezoelectric composites. Constr Build Mater 94:678–683
39. Topolov VYu, Bowen CR, Ermakov IA (2016) Remarkable hydrostatic piezoelectric response of novel 2–0–2 composites. Ferroelectr Lett Sect 42:90–95
40. Topolov VYu, Ermakov IA (2016) Piezoelectric properties and hydrostatic parameters of the novel 2–0–2 composite based on a relaxor-ferroelectric single crystal. Nano- i Mikrosistemnaya Tekhnika 18:696–699
41. Huang JH, Kuo W-S (1996) Micromechanics determination of the effective properties of piezoelectric composites containing spatially oriented short fibers. Acta Mater 44:4889–4898
42. Chan HLW, Unsworth J (1989) Simple model for piezoelectric ceramic/polymer 1–3 composites used in ultrasonic transducer applications. IEEE Trans Ultrason Ferroelectr Freq Control 36:434–441
43. Topolov VYu, Bisegna P (2010) Anisotropic piezoelectric properties of 1–3 ceramic/polymer composites comprising rods with elliptic cross section. J Electroceram 25:26–37
44. Bezus SV, Topolov VYu, Bowen CR (2006) High-performance 1–3-type composites based on $(1 - x)$ $Pb(A_{1/3}Nb_{2/3})O_3 - xPbTiO_3$ single crystals (A = Mg, Zn). J Phys D Appl Phys 39:1919–1925

45. Topolov VYu, Krivoruchko AV, Bisegna P, Bowen CR (2008) Orientation effects in 1–3 composites based on $0.93Pb(Zn_{1/3}Nb_{2/3})O_3$–$0.07PbTiO_3$ single crystals. Ferroelectrics 376:140–152
46. Topolov VYu, Bowen CR, Bisegna P, Krivoruchko AV (2015) New orientation effect in piezo-active 1–3-type composites. Mater Chem Phys 151:187–195
47. Topolov VYu, Bowen CR, Bisegna P (2015) New aspect-ratio effect in three-component composites for piezoelectric sensor, hydrophone and energy-harvesting applications. Sens Actuators A – Phys 229:94–103
48. Topolov VYu, Bowen CR, Bisegna P, Panich AE (2015) Effect of the matrix subsystem on hydrostatic parameters of a novel 1–3-type piezo-composite. Funct Mater Lett 8:1550049
49. COMSOL, Inc. (2007) COMSOL Multiphysics™ User's Guide (version 3.4). http://www.comsol.com/
50. Bowen CR, Topolov VYu, Isaeva AN, Bisegna P (2016) Advanced composites based on relaxor-ferroelectric single crystals: from electromechanical coupling to energy-harvesting applications. Cryst Eng Comm 18:5986–6001
51. Topolov VYu, Turik AV (2001) On increasing the hydrostatic sensitivity of three-component piezocomposites. Tech Phys Lett 27:81–83
52. Topolov VYu, Turik AV (2001) Porous piezoelectric composites with extremely high reception parameters. Tech Phys 46:1093–1100
53. Panich AE, Topolov VYu, Glushanin SV (2006) High-performance 1–3-type relaxor-ferroelectric-based composites. In: Vibroengineering, 6th international conference proceedings, October 12–14, 2006. Kaunas University of Technology, Lithuania. Technologija, Kaunas, pp 226–230
54. Topolov VYu, Panich AE (2009) Problem of piezoelectric sensitivity of 1–3-type composites based on ferroelectric ceramics. Ferroelectrics 392:107–119
55. Topolov VYu, Krivoruchko AV, Bisegna P (2011) Electromechanical coupling and its anisotropy in a novel 1–3–0 composite based on single-domain $0.58Pb(Mg_{1/3}Nb_{2/3})O_3$–$0.42PbTiO_3$ crystal. Compos Sci Technol 71:1082–1088
56. Dunn ML, Taya M (1993) Electromechanical properties of porous piezoelectric ceramics. J Am Ceram Soc 76:1697–1706
57. Glushanin SV, Topolov VYu (2001) Features of electromechanical properties of piezoelectric composites with elements of connectivity 1–1. J Phys D Appl Phys 34:2518–2529
58. Glushanin SV, Topolov VYu (2001) Anisotropy of the electromechanical properties and a high piezoelectric sensitivity of the 1–1 type ferroelectric piezocomposites. Tech Phys Lett 27:626–628
59. Topolov VYu, Bisegna P, Bowen CR (2011) Analysis of the piezoelectric performance of modern 0–3-type composites based on relaxor-ferroelectric single crystals. Ferroelectrics 413:176–191
60. Filippov SE, Vorontsov AA, Topolov VYu, Brill OE, Bisegna P, Panich AE (2014) Features of the piezoelectric effect in a novel PZT-type ceramic/clay composite. Ferroelectr Lett Sect 41:82–88
61. Bowles JE (1996) Foundation analysis and design. McGraw-Hill, New York
62. Balkevich VL (1996) Technical ceramics. Stroyizdat, Moscow (in Russian)
63. Glushanin SV, Topolov VYu (2005) Features of the electromechanical properties of 0–3 composites of the $Pb(Zr, Ti)O_3$-based ferroelectric ceramics – polymer type. Tech Phys Lett 31:346–348
64. Bowen CR, Topolov VYu (2003) Piezoelectric sensitivity of $PbTiO_3$-based ceramic/polymer composites with 0–3 and 3–3 connectivity. Acta Mater 51:4965–4976
65. Borzov PA, Vorontsov AA, Topolov VYu, Brill OE (2016) Piezoelectric performance and features of microgeometry of novel composites based on ferroelectric ZTS-19 ceramics. In: Parinov IA, Chang S-H, Topolov VYu (eds) Proceedings of the 2015 International Conference on "Physics, Mechanics of New Materials and Their Applications", Devoted to the 100th Anniversary of the Southern Federal University. Nova Science Publishers, New York, pp 115–122